

OXIDATION KINETICS OF 2.5 Cr-1Mo STEEL IN AIR, OXYGEN AND OXYGEN-WATER VAPOUR MIXTURE

A Thesis Submitted
in Partial Fulfilment of the Requirements
for the Degree of

MASTER OF TECHNOLOGY

By
A. S. KHANNA

08000

to the

DEPARTMENT OF METALLURGICAL ENGINEERING
INDIAN INSTITUTE OF TECHNOLOGY KANPUR

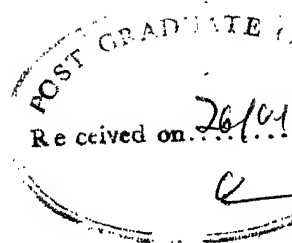
MAY, 1980

I.I.T. KANPUR
CENTRAL LIBRARY

Acc. No. A 62326

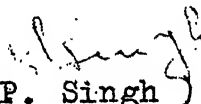
25 MAY 1980

ME-1980-M-KHA-OXI

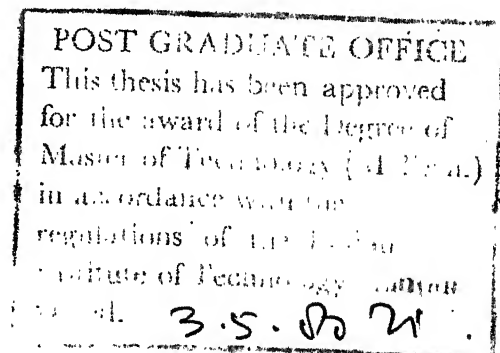


CERTIFICATE

Certified that the work contained in this thesis, entitled 'Oxidation kinetics of 2.5 Cr - 1 Mo steel in air, oxygen and oxygen-water vapour mixture' has been carried out by Mr. A.S. Khanna under my supervision and the same has not been submitted elsewhere for a degree.


(K.P. Singh)
Professor

Department of Metallurgical Engineering
Indian Institute of Technology,
Kanpur-208016



ACKNOWLEDGEMENTS

I feel great pleasure in expressing a profound sense of gratitude to Professor K.P. Singh for his constant cooperation, inspiration, encouragement and his kind, able and dynamic guidance during the course of this work.

I take this opportunity to express a deep sense of respect and sincere thanks to Dr. T.R. Ramachandran, Dr. K.P. Gupta and Dr. K.N. Rai for their valuable ideas on various topics related to the work embodied in this thesis.

I wish to express sincere thanks to Mr. M.N. Mungole for his constant effort to keep the lab. upto date and his unfailing help at every stage of this work.

I express my most humble thanks to Mr. K.P. Mukherjee of Physical Metallurgy, Mr. Das, Incharge of TEM Lab, Mr. Pande of X-ray laboratory, Mr. Bhatnagar of ACMS for their assistance in various measurements.

My appreciation towards the facilities extended by Central Workshop and Glass-Blowing section are duly recorded.

I must express my sincere thanks to Dr. V.S. Raghunathan and Mr. S. Vaidyanathan of RRC for their help in SEM and EDAX work..

I thankfully acknowledge the Department of Atomic Energy and specially to Dr. Placid Rodriguez for his kind efforts in offering me this opportunity to do M.Tech. at I.I.T. Kanpur.

In the end, I thank Mr. M.R. Nathwani for his careful and efficient typing of the thesis, Mr. B.P. Suman for carrying out cyclostyling work and Mr. V.P. Gupta for sketching the tracings.

My acknowledgements remain incomplete unless I gratefully mention, the patience, understanding and the help in various ways provided by my wife 'PREETI'.

A.S. KHANNA

CONTENTS

CHAPTER		PAGE
	ABSTRACT	
1	INTRODUCTION	1
2	EXPERIMENTAL	
	2.1 Materials	28
	2.2 Gases	28
	2.3 Specimen Prepration	29
	2.4 Weight gain measurements	30
	2.5 Examination of oxidation products	35
3	THERMOGRAVIMETRY	38
	3.1 Effect of temperature and time	51
	3.2 Effect of surface finish	57
	3.3 Effect of cold work on oxidation rate	59
	3.4 Effect of oxygen pressure	61
	3.5 Reproducibility of thermogravimetric results	63
	3.6 Effect of medium on the oxidation rate	64
	3.7 Activation energies	69
	References	72
4	EXAMINATION OF OXIDATION PRODUCTS	
	4.1 Physical Features	73
	4.2 Optical Microscopy	75
	4.3 Scanning Electron Microscopy	80

CHAPTER	PAGE
4.4 EDAX	82
4.5 X-ray Diffraction	86
4.6 Electron Microscopy	95
5 GENERAL DISCUSSIONS AND CONCLUSION	98
6 NEED OF FUTURE WORK	104
APPENDIX 1 Basic informations about samples (Tables 1 to 4)	
Thermogravimetric Data (Tables 5 to 9)	
APPENDIX 2 X-ray Diffraction Data for some important compounds.	
Colours of some important compounds.	

LIST OF FIGURES

Figure		Page
1.1	Iron oxygen phase diagram.	4
1.2	Mechanism of iron oxidation.	6
2.1	Reaction chamber and weight gain recording unit.	31
2.2	Gas train	34
3.1	Simultaneous DTA and TGA curve	39
3.2-3.4	Weight gain curves (linear plots)	42-44
3.13-3.14	Weight gain curves	65-66
3.5-3.7	Double log plots	45-47
3.8-3.9	Square of weight gain vs time plots	52-54
3.10	Single log plot	55
3.11	Effect of surface finish	58
3.12	Effect of oxygen pressure	62
3.15	Arrhenius plot	70
4.1-4.20	Optical micrographs	76-79
4.21-25	SEM ' '	81
4.26-4.28	EDAX Results	83-85
4.29-4.33	TEM Results	96

ABSTRACT

Oxidation behaviour of 2.5 Cr - 1 Mo steel was studied in air, oxygen and oxygen water vapour mixture. Isothermal runs were carried out at 1 atm pressure at various temperatures, ranging from 500°C to 1000°C. Rate laws were determined at each temperature and activation energies were thus calculated. Effect of time, temperature and medium on oxidation rate has been described.

Effect of surface finish, cold work and oxygen pressure on oxidation rate was also determined.

Oxidation products have been examined, systematically using optical microscopy, SEM, EDAX and X-ray Diffraction. Few oxide layers were also observed in TEM.

CHAPTER 1.

INTRODUCTION

Chromium-Molybdenum steels have been found to be useful materials for steam-generating components of various power reactors. Therefore a good amount of work has been published about the compatibility of these steels with steam¹⁻³. Previously these steels were being used in gas-cooled reactors, where carbon dioxide gas was used as coolant. Hence many workers⁴⁻⁷ have studied in detail the corrosion and oxidation characteristics of these steels in carbon dioxide. A number of papers^{8,9} have also been published, where the mechanical properties of these steels have been discussed in detail. An extended review¹⁰ covering various aspects of chrome-moly steels was published in 1974. However, very few publications appeared in literature which can highlight the oxidation characteristics of these steels in air and oxygen. Present work has been carried out keeping this in view.

Oxidation kinetics of 2.5 Cr - 1 Mo steel have been studied in air, dry oxygen and oxygen water vapour mixture between temperature ranging from 500°C to 1000°C. The analysis of the oxidation products formed has also been carried out systematically using optical microscopy, SEM, EDAX and X-ray diffraction.

An extensive literature survey on the oxidation characteristics of pure iron, chromium, molybdenum and their alloys was made and is summarized below.

OXIDATION OF PURE IRON:

Iron is one of the most important metal which has been studied quite immensely and elaborately. Oxidation of this metal has been studied from room temperature to as high as 1100°C . These studies have been carried out in various environments like air, oxygen, water vapours, steam, carbon dioxide etc. A brief summary of the oxidation behaviour of this metal in these environments will be given here.

Room temperature oxidation of iron has been reported by many workers^{11,12}. According to Gilroy et al.¹², film growth in air formed oxide on pure iron follows the inverse rather than direct logarithmic relationship.

Above 250°C and at normal pressure of air or oxygen, the oxidation rate of iron has been found frequently to be parabolic¹³⁻²⁰. Stanley¹⁸ expressed the parabolic rate constant between temperature 500°C to 1100°C by an equation $K_p = 0.37 \exp (-33,000/RT) \text{ g}^2 \text{ cm}^{-4} \text{ sec}^{-1}$. On observing the dependence of parabolic rate constant on temperature, one notes a break at $500-600^{\circ}\text{C}$, which is due to the fact that

FeO is not stable in bulk below 570°C , according to the iron-oxygen equilibrium diagram shown in Fig. 1.1, although it may continue to be present in the form of thin film adjacent to the iron surface down to 400°C ^{21,22}.

Iron forms three stable oxides, Wustite, FeO, magnetite, Fe_3O_4 and hematite, Fe_2O_3 . FeO is a p-type conductor. The defects consist of vacant cation sites and equivalent number of electron defects represented chemically by trivalent Fe^{3+} ions. Consequently diffusion is essentially cationic via vacant cation sites. The diffusion ratio is relatively high. Fe_3O_4 , also exists with an excess of oxygen, but the excess is much smaller than with Wustite, and the defect concentration correspondingly less. It follows from marker diffusion measurements by Birchenall and his Colleagues^{17,23} that both cations and anions diffuse in Fe_3O_4 . Hematite is an n-type conductor²⁵ in which anions largely diffuse¹⁷.

Effect of oxygen pressure on the oxidation of iron was studied by Caplan et al.¹⁵ at 500°C . They found that oxidation was lower at 10 torr than at 760 torr owing to greater separation between oxide and metal. It is reported²⁰, that at $900\text{--}1000^{\circ}\text{C}$ if oxygen pressure exceeds 1-20 mm Hg a transition from linear to parabolic oxidation takes place.

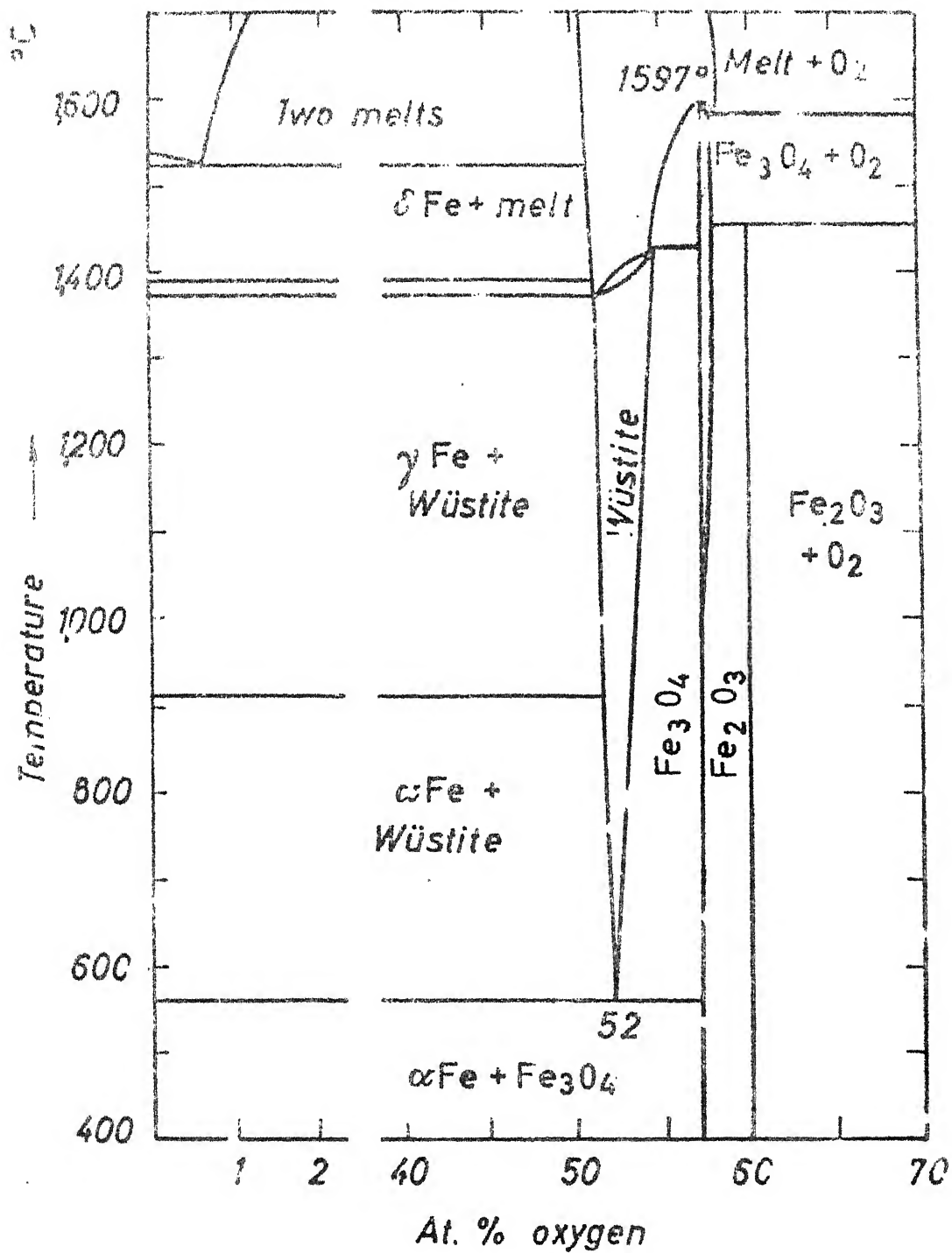


Figure 1-1 Equilibrium diagram of the iron-oxygen system.

Under these conditions, Fe_3O_4 and Fe_2O_3 are formed on the top of the Wustite and oxidation becomes diffusion controlled. Hauffe²⁷ reduced the oxygen potential in the gas phase by using CO/CO_2 mixtures. In this case scale formed at $900\text{--}1000^\circ\text{C}$ consisted only of FeO . They found that under these conditions the oxygen uptake was linearly proportional to time, although compact scale free of voids was formed. The oxidation rate was found to depend on gas pressure in the following manner:

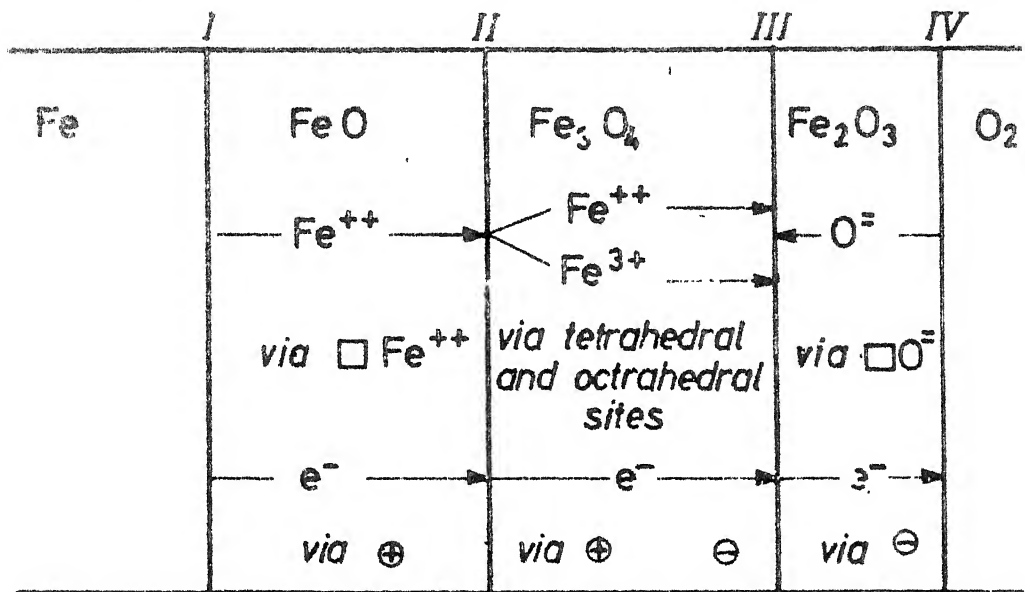
$$K_1 = \text{const.} (p_{\text{CO}_2}/p_{\text{CO}})^{0.71}$$

Pfeiffier²⁶ studied the oxidation of iron at (10^{-3} - 1 mm Hg) established by $\text{Cu}_2\text{O}-\text{CuO}$ equilibrium and found that in this case only FeO was formed and obtained the linear rate constant K_1 varying with oxygen pressure as:

$$K_1 = \text{const.} p_{\text{O}_2}^{0.7}$$

From all these observations, the simplified picture shown in Fig. 1.2 emerges for the oxidation mechanism of iron above 600°C as given by Hauffe²⁷.

Below 700°C , the relative proportion of Wustite and magnetite in the scale does not appear to remain constant with time, but Fe_3O_4 is present in decreasing proportions²⁹.



Phase boundary reactions:

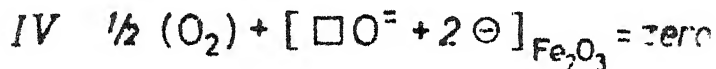
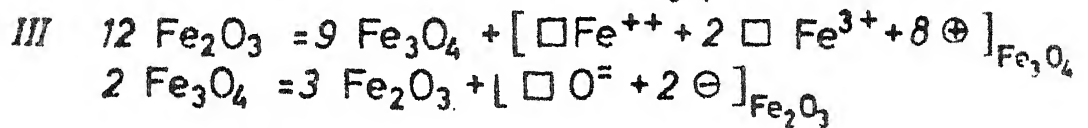
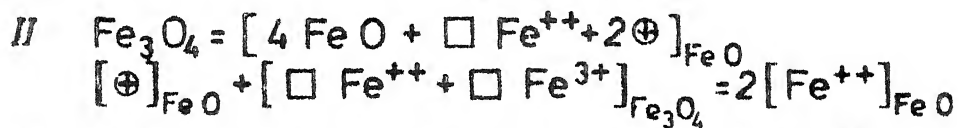
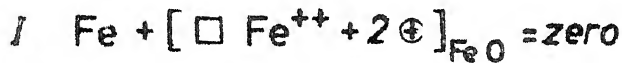


Figure 1.2 Oxidation mechanism of iron above 600°C after HAUFFE.

Below 570°C , Wustite disappears almost entirely. Since oxygen diffuses predominantly in Fe_2O_3 and to some substantial proportion in Fe_3O_4 ¹⁷, it may now reach the interface and even penetrate the metal. This was, in fact concluded by Vernon et al³⁰ from various low temperature investigations. These workers showed that the thickness of strippable film remained approximately constant for oxidation times varying from 20-450h at 180°C , the weight increase of the specimens being due to oxidation on existing oxide inclusions beneath the Strippable film. At 225°C , however, the oxygen absorbed resulted in progressive thickening of the strippable oxide film. Thus there appears to be a pronounced change in the mechanism of the oxidation of iron at about 200°C . Above this temperature, oxidation is essentially parabolic, below it becomes logarithmic³⁰⁻³². At low temperature obviously thin film mechanisms apply. The driving force for the ionic movement across the oxidation layer is not a concentration gradient but an electric field as in the Mott-Mauffe-Il'schnev model³³.

Oxidation of pure iron has been studied widely in presence of watervapours or steam³⁴⁻³⁷. Presence of steam accelerates the oxidation in oxygen of mild steel and two grades of pure iron of varying purity. Rahmel et al.³⁵ reported that the scaling rate of iron is not influenced by

water vapours at 750°C . At 850°C the rate rises by a factor of 1.2, at 950°C by a factor of 1.6 respectively, in presence of water vapour. They presumed that pores occur at the iron-wustite interface during the oxidation. In the presence of water vapour, a $\text{H}_2/\text{H}_2\text{O}$ mixture is formed in these pores which transports by an oxidation reduction mechanism, oxygen to the iron surface. Therefore oxide bridges are built up from the metal to scale, which enables the further oxidation of the metal without substantial inhibition.

Caplan et al.³⁸ studied the oxidation of cold worked and annealed iron at 500°C and 550°C in O_2 at 1 atm. pressure. They observed that apparent parabolic rate constant for cold worked Fe was high initially and dropped steeply and approached constant value at long times. Annealed iron oxidised slowly and developed voids between oxide and metal. Caplan and Cohen³⁹ in 1967 observed that cold work increased the oxidation rate of iron in water vapour. According to them cold work metal surface provides sinks thereby minimising interfacial detachment.

Oxidation of Chromium:

Oxidation of pure chromium has been studied quite widely by various workers. The literature on the resistance

of unalloyed Cr to oxidation has been summarized to 1960 by Kubaschewski and Hopkins³³ and Ignatove and Shanguhova⁴⁰. Hagel⁴¹ reported the scaling of Cr in oxygen and air at 700 to 1100°C. Widmer et al⁴² heated Cr in oxygen and air at 980 to 1200°C, Fox and McGurty⁴³ in air at 1260°C, and Wilms and Rea⁴⁴ in air at 1038°C. Caplan et al.⁴⁵ oxidised Cr in 1 atm of oxygen at 980, 1090 and 1200°C for periods upto 100 hrs. Mortimer and Post⁴⁶ in 1968 did an extensive study on the oxidation of pure chromium in oxygen under isothermal conditions in range of 650 to 1000°C for periods upto 1200h.

The only oxide formed on heating Cr in oxygen at various temperatures is Cr_2O_3 ^{22,48}. Electron diffraction lines are sharp when the oxide is formed above 600°C and diffuse for lower temperatures. X-ray examination shows that Cr_2O_3 is also formed on heating the metal in air^{49,50}, but at high temperatures at least, some nitrogen is taken into solution, and this separates as Cr_2N on cooling in air, but is retained in solution on quenching in water. According to Arkharov et al.⁴⁹ the oxidation rate in air is less than that in pure oxygen Cr_2O_3 is p-type semiconductor⁵¹ hence metal additions of higher valency than three seem to increase, additions of lower vacancy decrease the oxidation

rate of chromium. According to Gulbransen et al⁵² pure Cr oxidised more slowly than a less pure one.

Oxidation kinetics of Cr in pure oxygen has been described by Mortimer and Post⁴⁶, in various stages. According to them in 0-2h oxidation a parabolic rate equation was obeyed and they found the activation energy of this process as 59.5 Kcal/mole. During 2-20h, the oxidation rate continued to decrease steadily but after 2-5h the weight increase was always less than that predicted by the rate equation derived for 0-2h period. Instead the data for 5-20h period fitted a parabola with lower rate constant. The most interesting results were found during 1200 h oxidation at 950°C. During this, sudden increases in oxidation rate observed from time to time. The first break appeared was during 60-80 hrs and the weight change was around 2.5 mg/cm². Five such breaks were observed during 1200h isothermal oxidation.

Thus, according to Mortimer and Post⁴⁶ high purity Cr oxidises by a diffusion controlled process during the first few hours^{of} oxidation in the range 650-950°C. The rate constants are in agreement with values for cation diffusion in Cr₂O₃. Blistering and cracking of the scale occurs at 950°C. The scale on Cr is most susceptible to cracking but the origin of stresses is not fully understood. However

the stress appears to be an intrinsic feature of the oxidation mechanism and the blistering is apparently greatest in the finest grained scale. Further the oxidation of chromium is remarkably dependent upon experimental technique.

According to Caplan⁴⁵ behaviour of Cr in high temperature service could be improved if the rapid initial oxidation rate was avoided and if anion diffusion rate was suppressed.

Caplan⁴⁵ showed that moisture does not significantly affect the oxidation of chromium. They observed the close correspondance between weight gain time curves for etched Cr oxidised in wet and dry oxygen at 1090°C upto 100 hr.

Oxidation of Molybdenum

Oxidation of Molybdenum has been extensively investigated in late fifties and early sixties, because of its very attractive mechanical properties at temperatures well above those covered by conventional creep-resisting alloys.

Quantitative study of the oxidation of Mo has been pursued by a number of investigators⁵³⁻⁵⁹. Molybdenum remains bright upto 200°C during a 2h exposure to air⁶⁰, it tranishes to a steel-blue colour at 300°C and forms adherent oxide at temperatures upto 600°C. Above this the outer layer of MoO₃ becomes granular⁶¹, then melts and volatilizes so that the rate of oxidation is very high and occurs with a net loss in weight⁶⁰⁻⁶⁴.

Gulbransen and his Co-workers^{53,54} measured the rate of oxidation in the pressure range 10^{-6} to 76 mm Hg of oxygen. A substantial increase in oxidation rate was observed with an increase of either temperature or pressure. At low pressure and times less than an hour, Mo oxidises according to a parabolic rate law. Below 450°C the oxide formed as a thin surface film is MoO_3 , above 450°C , MoO_2 forms with an associated increase in oxidation rate, with extended test times the oxidation curve deviates from the parabolic, although the coatings remain partially protective. The rate constants⁵³ for the parabolic oxidation of Mo and Fe at 7.6 cm of oxygen pressure and 450°C are 3.33×10^{-13} and $0.334 \times 10^{-13} \text{ gm cm}^{-2} \text{ sec}^{-1}$ respectively.

Peterson and Fassell⁵⁸ studied the oxidation of Mo at high pressures (1-47.6 atm O_2) in the temperature range 500°C to 700°C . The only oxidation product observed under these conditions was MoO_3 . Above 525°C the oxidation rate becomes sensitive to pressure, increasing with an increase in pressure, at nearly all temperatures and pressures the oxidation is linear indicating a non-protective coating. However at temperature between 650°C and 700°C a parabolic oxidation rate was observed by these investigators at low pressures, changing gradually to a linear rate at higher pressures.

Lustman⁵⁶ reports that data prior to 1950 on the oxidation of Mo in air as a function of temperature are scanty. He noted that the oxidation rate not only increases with temperature but that during the course of a test at a given temperature, it also may increase with time. Lustman also reported that above the m.p. of MoO_3 , 795°C an essentially constant rate of oxidation was observed.

Simnad and Spiliners⁵⁹ have studied the mechanism of oxidation of Mo in pure O_2 at 1 atm. in temperature range 500°C to 700°C . They found that vaporization of MoO_3 from the surface of an oxidising specimen into pure oxygen at 1 atm. is linear with time, with an activation energy of 53,000 cal/mole below 650°C and 89,600 cal/mole at temperature above 650°C . They found that at low temperatures the formation of MoO_3 is parabolic and at higher temperature is linear. The suboxide MoO_2 thickness does not increase beyond a very small critical thickness. At temperatures above 725°C catastrophic oxidation of an autocatalytic nature was encountered by them.

In a later study by Jones et al.⁶⁵ of Mo in air, they found that initially the oxidation is parabolic changing ultimately to a constant rate. The detailed character of the oxidation curve depends on time, temperature and sample history. According to them oxidation of Molybdenum

from the surface inward is a rate process and not an equilibrium process, therefore it would be expected that several layers of oxide would co-exist on the Mo surface. Surface phases such as

Molybdenum metal	Molybde- num saturated with O_2	Lower oxides of Molybdenum	MoO_3
---------------------	--	----------------------------------	---------

Can be inferred from the gradient of oxygen activity. By X-ray diffraction analysis and metallographic study on some sheet sample oxidised at $571^\circ C$, they were able to show three phases consisting of MoO_3 the outer oxide layer, MoO_z ($3 > z < 2$) adjacent to the unoxidised metal core and $MoO_{z'}$ ($3 > z' < z$) at places where MoO_3 got ruptured. With the help of marker studies they indicated that oxidation is initiated and then proceeds at the metal interface through diffusion of oxygen ions (O^{--}) to the metal oxide interface.

In air saturated with H_2O vapours, Friedrich⁶⁶ reported that hydrous molybdenum oxide formation takes place, which follows a linear law, rate constant for which is $0.27 \text{ gm cm}^{-2} \text{ day}^{-1}$.

Iron-Chromium Alloys

A recent study of the oxidation of pure iron and iron-chromium alloys containing 0.2-10.0 pct. chromium in oxygen at 750-1025°C shows that whereas the former follows parabolic 'law' the latter obeys no simple reproducible growth relation. At very low chromium contents, the alloy oxidizes more rapidly than iron initially, but for longer periods rate is less. As the chromium content is increased the oxidation rate falls at any given temperature.

The mechanism of oxidation is probably essentially the same in oxygen, air, water vapour and carbon dioxide, namely the break-through of an initially protective ' Cr_2O_3 ' rich layer followed by scale growth. However, the actual rate may show considerable variation. It is reported⁶⁹ that oxidation rate is often slower in air. Most studies have been conducted in dry oxygen^{67,68,70-80} or air that is substantially dry^{71,76,78,81-83}. Somewhat similar behaviour is observed in the two environments but the growth rate in the initial stages and the eventual break-through is appreciably faster as the partial pressure of oxygen is increased⁷¹. While comparing results obtained in oxygen to air, one should be careful because difference may not be entirely due to variation in oxygen partial pressure. Compounds such as

Cr_2N may be formed under some conditions^{69,84} and nitrogen may be trapped in the ' Cr_2O_3 ' lattice. Two N^{3-} ions replacing three O^{2-} ions would tend to make the ' Cr_2O_3 ' more nearly stoichiometric, so cutting down the oxidation rate. In almost all cases, water vapours in small or large quantities increase the scaling rate of pure Fe-Cr alloys⁸⁵⁻⁸⁶. Probably the main reasons for the rate differences are again connected with the influence of atmosphere on the ' Cr_2O_3 ' defect structure. In water vapour atmosphere, the film is effectively being produced at a lower oxygen potential and may also contain H^+ and OH^- ions. According to Wood⁸⁷ a slightly cation-deficient ' Cr_2O_3 ' lattice in presence of OH^- ions in place of O^{2-} ions would effectively increase the number of cation vacancies and hence the growth rate. It is also significant that in water vapour oxidation, appreciably more ' FeO ' is formed and ' Fe_2O_3 ' is generally absent. The absence of or reduced quantities of the less ductile ' Fe_3O_4 ' and ' Fe_2O_3 ' may make some contribution to the increased rates⁸⁸.

Pure iron-chromium alloys containing over 13 pct. Cr are in equilibrium with Cr_2O_3 containing little dissolved Fe_2O_3 , at least at 1000°C and 1300°C ⁷⁷. Alloys of lower chromium content are in equilibrium with $\text{Fe Fe}_{(2-x)}\text{Cr}_x\text{O}_4$ ($0 \leq x \leq 2$). Diffraction techniques^{76,89} and EPMA prove that inner layers of nodules contain principally a mixture

of chromium oxide and iron oxides and the outer regions almost pure oxides of iron. In the completely stratified scales various combinations of ' Cr_2O_3 ' ' $\text{Fe Fe}_{(2-x)}\text{Cr}_x\text{O}_4$ ' rich in chromium, ' FeO ', ' Fe_3O_4 ' and ' Fe_2O_3 ' may appear, usually in this order from the alloy to the outer surface, depending upon the conditions^{67,68,71}. EPMA of scales produced on Fe-14.4 pct. Cr alloys in steam at 950-1000°C clearly reveal two major scale layers, the outer one consisting largely of ' FeO ' and the inner one containing a rather complex distribution of oxides of iron and chromium⁹⁰. Many other workers⁷⁸ have also shown increased Cr content near alloy oxide interface.

During oxidation underlying alloy is depleted with respect to Cr and with respect to certain other alloying elements in the case of complex alloys. For Fe-14.4 pct. Cr oxidised in steam for 10-30 min, there is a 5-micron wide layer showing depletion, the minimum recorded⁹⁰ being 11.5 pct. Cr. The appreciable depletion is related to large activation energy of inter diffusion of iron and Chromium⁹¹. It appears, currently accepted theories on the vacancy mechanism of diffusion do not easily explain diffusion rates in the Fe-Cr alloys. Ring diffusion or some other mechanism may be involved at some compositions⁹². Another important investigation⁹³, the influence of adding 10 pct. of third

element on diffusion of Cr in Fe was studied at 950-1000°C. Sn increases the rate, W and Ni have little effect and Ti, Si, Nb and Be reduce the rate by a half to a tenth.

When the Cr content of an Fe-Cr alloy is very low, the alloy should scale in much the same way as pure iron except that the thickness, composition and mechanical properties of the 'FeO', ' Fe_3O_4 ' and ' Fe_2O_3 ' layers will be affected by the Cr. The observation that in the initial stages Fe-0.2 pct. Cr oxidises more rapidly than Fe in oxygen⁶⁷ could be explained by the fact that Cr present in the FeO making it even more cation deficient. It seems then that the reduced rates of oxidation of low Fe-Cr alloys as compared with iron are due to the presence of $\text{Fe Fe}_{(2-x)}\text{Cr}_x\text{O}_4$ spinel and to the decreased amount of FeO formed⁶⁷.

Oxidation rates are affected to a greater or lesser extent by the presence of other alloying and 'tramp' elements. Oxides of these elements, distributed in the bulk oxide in solid solution or as discrete layers or particles, may affect the defect structure and conductivity and hence the growth rate of scale and its mechanical properties, in particular its adhesion to the alloy and its plasticity. Here only the effect of Mo will be mentioned.

Mo is enriched in passive films formed at room temperatures^{93,94} small quantities of this element may be

tolerated in stainless steels at high temperatures but larger quantities of this element can lead to catastrophic destruction of the oxide^{82,95}. The situation appears to depend on the Mo and Cr contents and on the temperature. The location of the Mo within the scale may be important Ralph⁹⁶ recently has suggested various alloys formed by combination of chromium and Mo which have excellent corrosion resistance. For example 18 Cr - 2 Mo steel has corrosion resistance at least comparable and frequently superior to that of AISI type 304, 26 Cr - 1 Mo steels provide outstanding performance in caustic environment and 29 Cr - 4 Mo steels provide extraordinary corrosion resistance.

Iron-Molybdenum Alloys

Rahmel⁹⁷ and coworkers studied the oxidation of Fe-Mo alloys (Mo content from 0.5-5.6 wt pct.) in air at temperature range from 500-1000°C. They concluded that presence of Mo reduces the oxidation rate of Fe by almost a power of 10. Scale on Fe-Mo alloys is built up of 3 layers between 500-620°C. Below the outer layers of hematite and magnetite a thin layer of $\text{Fe}_4\text{Mo}_6\text{O}_{16}$ lies directly above the metal. Between 620°C and 700°C the scale is again built up of 3 layers but instead of $\text{Fe}_4\text{Mo}_6\text{O}_{16}$ below the outer layers, a 2-phase layer built up of Wustite and the spinel Fe_2MoO_4

was detected. Above 700°C the scale is built up of 4 layers which differs from the layers formed at $620-700^{\circ}\text{C}$. In that, between the magnetite layer and the inner 2-phase layer, a closed Wustite layer is formed. The reduction of oxidation rate is due to the formation of inner Fe-Mo-O compound. Since diffusion coefficient of Fe in compound Fe_2MoO_4 or $\text{Fe}_4\text{Mo}_6\text{O}_{16}$ are very likely to be smaller than Wustite or magnetite. Mo is accumulated in the inner most layer while the outer layers are almost free of Mo.

Vladimirova et al.⁹⁸ studied the oxidation of Fe-5 pct. Mo and Fe-10 pct. Mo alloys in air between temperature range 600 to 900°C . The apparant activation energy for 5 pct. Mo alloy was found to be 39685 cal/mole and that for 10 pct. Mo alloy was 40,535 cal/mole. They expressed the oxidation process for 50 pct. alloy at $700-900^{\circ}\text{C}$ by equation

$$\log K = - 39,685/4.57T + 7.64$$

and for 10 pct alloy as

$$\log K = - 40,535/4.57T + 8.04$$

where K is the rate constant.

As found by the previous author⁹⁶ the top layer was Fe_2O_3 the middle Fe_3O_4 and inner layer was perous FeO with Mo inclusion. Due to the slow diffusion of Mo in comparison to O and Fe, Mo accumulates in the inner layer of oxide.

References:

1. M.I. Manning and E. Metcalf, Brit. Nuc. Energy Soc. Conf. on ferritic steels for fast reactor steam generators, London, June 1977.
2. Oxidation of ferritic steels - TRG - Report - 2996(R).
3. J.C. Ralph et al., 6th Int. Conf. on heat transfer, Utah 14-17 Aug. 1977 Proc. Vol. 4, 1978, pp. 379-384.
4. Brit. Corr. J. Jan. 1968, 3, (1), 34-46.
5. Trans. of Brit. Nuc. Soc., March 1974.
6. J. of electrochemical Soc. 1976.
7. P.L. Harrison et al., Mat. Sc. 1976, 10(1), 220-233.
8. J. Iron and Steel Inst. of Japan, 1971, 52(2), 367-385.
9. Iron Steel, 1956, 29(1), P 150-153.
10. Review on Chrome-Moly Steels, GEAP-20589, Oct. 1974.
11. Brit. Corr. J. Jan., 1968, 3(1), 34-46.
12. J. of Iron and Steel Inst. Japan, 1971, 52(2), 367-385.
13. N.B. Pilling and R.E. Bedworth, J. Inst. Met. 29 (1923) 529.
14. W.H.J. Vernon, Trans. Faraday Soc. 31 (1935) 1668.
15. A.B. Winterbottom, J. Iron Steel Inst. 165 (1950) 9.
16. J. Paidassi, Acta Metallurgica, 6(1958) 184.
17. M.H. Davies et al., J. Metals, N.Y. 3 (1951) 8895 (1953) 1250.

18. J.K. Stanley et al., Trans. Amer. Soc. Metals 43 (1951) 426.
19. A. Portevin et al., Rev. Metall. 31 (1934) 101, 186.
20. N.G. Schmahl et al., Arch Eisenhüttenw. 29 (1958) 147.
21. E.A. Gulbransen and R.J. Ruka, J. Metals N.Y. 188 (1950) 1500.
22. E.A. Gulbransen and J.W. Hickman, Trans. Amer. Inst. Min. Engrs. 171 (1947).
23. L. Himmel et al., J. Metals, N.Y. 5 (1953) 827.
24. J.S. Anderson, Faraday Soc. Disc. 4 (1948) 163.
25. D. Caplan, M.J. Graham and M. Cohen, Corr. Sc., Vol. 10, 1970, p 1-8.
26. H. Pfeiffer and C. Laubmeyer, Z. Elektrochem, 59 (1955) 579.
27. K. Hauffe and H. Pfeiffer, Z. Metallk. 44 (1953) 27.
28. K. Hauffe, Metalloberfläche (A.) 8 (1954) 97.
29. J. Paidassi, Bol. Soc. Chil. Quim 5 (1953) 46.
30. W.H.J. Vernon et al., Proc. Roy Soc. (A) 216 (1953) 375.
31. O. Kubaschewski and D.M. Brasher, Trans. Faraday Soc. 55 (1959) 1200.
32. J. Moreau and M. Cagnet, Rev. Metall 55 (1958) 1091.
33. O. Kubaschewski and B.E. Hopkins 'Oxidation of Metals and Alloys' Ed. 1967, p. 75.

34. P.L. Surman, Corr. Sc. 1973, 13, p. 113-124.
35. A. Rahmel et al., Corr. Sc., 1965, 5, p. 333-346.
36. C.W. Tuck et al., Corr. Sc., 9 (1969) p. 271-287.
37. D. Caplan and ^{M. Cohen,} \angle Corr. Sc. 7 (1967) p. 725-727.
38. D. Caplan, G.I. Sproule and R.J. Hussey, Corr. Sc. 1970 (10) p. 9-17.
39. D. Caplan and M. Cohen, Corr. Sc., Oct. 1967, 7(10), 725-727.
40. D.V. Ignatov and R.D. Shamgunova, Mechanism of oxidation of Alloys with Nickel and Chromium as Base, P. 34, Izd-vo Akademii Nauk CCCP, Moscow (1960), p. 28 NASA Technical translation E.59 (March 1961).
41. W.C. Hagel, General Electric Research Lab. Report No. 62-RL-2917 M (Feb. 1962).
42. R. Widmer et al., Refractory Metals and alloys, Metallurgical Society conferences Vol. 11, p. 183, Interscience NY (1961).
43. J.E. Fox and J.A. McGurty, Metallurgical Society Conferences, Vol. 11, p. 207, Interscience, NY (1961).
44. G.R. Wilms and T.W. Rea, J. Less Common Metals 3, 234 (1961).
45. D. Caplan, AlmaHarvey and M. Cohen, Corr. Sc. (1963), 3, pp 161-175.

46. D. Mortimer and M.L. Post, *Corr. Sc.* 1968, (8), pp. 499-512.
47. *Workstoffe, Korrosion*, Nov. 1970, 21 (11) 886-94.
48. S. Miyake, *Sci. Pap. Inst. Phys. Chem. Res., Tokyo* 29 (1936) 167 31 (1937) 161.
49. V. Arkhrov et al., *Fiz. Metal. i Metalloved., Akad. Nauk, SSSR* 5 (1957) 190.
50. C. Phalnikar et al., *J. electrochem. Soc.* 103 (1956) 429.
51. G. Lorenz and W.A. Fisher, *Z. Phys. Chem. (NF)* 18 (1958) 265.
52. E.A. Gulbransen and K.F. Andrew, *J. Electrochem. Soc.* 104 (1957) 334.
53. J.W. Hickman and E.A. Gulbransen, *Met. Tech.* 14, TP 2144 (1947).
54. E.A. Gulbransen and W.S. Wysong, *ibid*, 14, TP 2226.
55. E.S. Jones 'A study of the oxidation characteristics of Molybdenum at elevated temperatures, M.Sc. thesis' The Ohio State Univ. 1952.
56. B. Lustman, *Met. Prog.*, 57, 629 (1950).
57. J.F. Mosher, *The kinetics of the oxidation of Molybdenum* M.Sc. Thesis, The Ohio State Univ. (1953).
58. R.C. Peterson and W.M. Fassell 'High Pressure oxidation of Metals' Mo in oxygen, Tech. Report VI DA-04-495 ORD-237, 1954.

59. M. Simand and A. Spilners. Trans. AIME 203, 1011 (1955).
60. E. Nachtigall, Z. Metallk. 43 (1952) 23.
61. A.A. Zaitsev and D.V. Ignatov, Izvest, Akad, Nauk. SSSR, Metally, 1970, (4), 218-221.
62. B. Lustman, Metal Progr. 57 (1950) 629.
63. O. Kubaschewski and A. Schneider, J. Inst. Met. 75 (1949) 403.
64. V. Akharov and Yu. D. Kozmanov, Fiz. Metal i Metalloved, Akad Nauk SSSR 11 (1956) 361.
65. E.S. Jones et al., Corrosion, 14 (1958) 2t.
66. K. Friedrich, J. Less Common metals, Oct. 1968, 16, (2), p. 147-156.
67. D. Lai et al., Metallurgy Rept. No. 22, Princeton Univ., 1960.
68. D. Lai et al., Corrosion 17, 109 (1961).
69. V.I. Arkharov et al, Fiz. Metal. Metalloved, Akad. Nauk SSSR 5, 190 (1957).
70. W.W. Smeltzer, Acta Met. 8, 268 (1960).
71. H.M. McCullough, M.G. Fontana and F.H. Beck, Trans. Amer. Soc. of Metals 43, 404 (1951).
72. E.J. Felton, J. Electrochem. Soc. 108, 490 (1961).

73. R.L. Rickett and W.P. Wood, Trans. Amer. Soc. Metals 22, 347 (1934).
74. D. Caplan, A. Harvey and M. Cohen, J. Electrochem. Soc. 108, 134 (1961).
75. H.H. Uhlig and A. De S. Brasunas, *ibid* 97, 448 (1950).
76. H.J. Yearian et al., Corr. 13, 597t (1957).
77. A.V. Seybolt, J. Electrochem. Soc. 107, 147 (1960).
78. H.J. Yearian et al., Corrosion 12, 515t (1956).
79. J. Moreau and J. Benard, C.R. Acad. Sci. Paris 237, 1417 (1953).
80. D. Caplan, J. Electrochem. Soc. 107, 359 (1960).
81. D. Caplan and M. Cohen, Trans. Amer. Inst. Min. Engrs. 194, 1057 (1952).
82. A. De S. Brasunas and N.J. Grant, Trans. Amer. Soc. Metals, 44, 1117 (1952).
83. S.S. Brenner, J. Electrochem. 102, 16 (1955).
84. C.A. Phalnikar et al. J. Electrochem. Soc. 103, 429 (1956).
85. C.T. Fujii and R.A. Meussner, N.R.L. Rept. 5506, 1960.
86. J. Benard, J. Moreau and J. Plateau, Z. Elektrochem. 61, 59 (1957).
87. G.C. Wood, Corr. Sc., 1961, Vol. 2, pp 173-196.
88. J.D. Mackenzie and C.E. Birchennall Corr. 13, 783t (1957).

89. J.F. Radavich, A.S.T.M. Special Publ. 171, 89 (1955).
90. G.C. Wood and D.A. Melford, J. Iron. St. Inst. 198, 142 (1961).
91. T.P. Hoar and E.A.G. Croom, J. Iron Steel Inst. 169, 101 (1951).
92. H.W. Paxton and E.J. Pasierb, Trans. Met. Soc. Amer. Inst. Min. Engrs. 218, 794 (1960).
93. E.M. Mahila and N.A. Nielsen, Trans. Electrochem. Soc. 93, 1 (1948).
94. T.N. Rhodin, Corrosion 12, 123t 465t (1956).
95. A.B. Wilder and J.O. Light, Trans. Amer. Soc. Metals 43, 323 (1951).
96. R.M. Davisen et al. Met. Prog., June 1979, 115, (6), pp. 40-46.
97. A. Rahmel et al., Arch Eisenhuttenw, 30, 351-360 (1959) Chem. Abs. 53, 16890.
98. M.G. Vladimirova et al., Trudy Leningrad, Lesotekh, Akad. im.S.M. Kirova 92, No. 3, 105-15, Chem. Abs. 56, 4470.

CHAPTER 2

EXPERIMENTAL

2.1 Materials

Exact chemical composition of the material, analysed for elements carbon, chromium and molybdenum was found to be:

Element	C	Cr	Mo
wt pct.	0.09	2.2	1.1

Above material in the form of 1 mm thick strips cut from a boiler tube by milling operation, was received from Metallurgy Division Reactor Research Centre, Kalpakkam.

2.2 Gases

For carrying out the oxidation in air, laboratory air was used. No purification or drying was carried out. For oxidation in oxygen environment, commercial grade oxygen cylinder was used. The gas was purified to remove the impurities like moisture and carbon dioxide, by passing it over sulphuric acid and soda asbestoes. The oxidation in oxygen-water vapour mixture was carried out by bubbling

the purified gas, as explained above over distilled water maintained at a constant temperature of 32°C . This gave oxygen gas saturated with about 5 pct. water vapours.

2.3 Specimen Preparation

Rectangular specimens of surface area ranging from $1\text{--}2\text{ cm}^2$ [exact details can be seen in Tables 1 to 4 in Appendix 1] were used throughout the experiment. These were cut from a .5 mm thick foil obtained by cold rolling of the 1 mm thick strips. The rectangular specimens were then mounted on a pyrex block using a double adhesive tape. One side of this specimen was polished upto 4/0⁰⁰ emery paper. After this, the other side was similarly polished upto 4/0⁰⁰ emery finish. The bright shining specimens so obtained were then sealed in quartz capsule under a vacuum of the order of 10^{-3} torr. These were then annealed at 850°C for two hours. Before final using, it was again rubbed on 4/0⁰⁰ emery paper in order to remove any oxide layer formed during annealing. The specimen was then washed with distilled water and acetone and finally dried.

Some of the specimens were prepared, by first annealing the thin strips at 850°C for two hours followed by cutting and polishing. This was done in order to find the effect of cold work (discussed elsewhere) on oxidation rate.

2.4 Weight Gain Measurements:

For weight gain measurements a continuous recording semimicro balance (manufactured by Ainsworth and Sons Inc., USA) was used. The set up is shown schematically in Fig. 2.1. It had an electronic indicating and recording device. With the help of an x-y recorder it gave a continuous record of the weight changes occurring in the sample as a function of time on a chart. The balance had a sensitivity of 0.1 mg, readability by estimation, of 0.01 mg and reproducibility of ± 0.03 mg. The span which is attached on the chart read 10 mg. Whenever the recorder pen approached a chart edge, a weight of exactly one full scale value was applied or removed to rescale the instrument. Enough weights for forty full span steps had been provided. The capacity of the balance was 100 gm. The zero stability of the instrument was fairly good.

The sample under investigation was suspended from the hook under the left pan of the balance. A platinum wire was used for suspending the specimen. In order to keep the wire straight, it was surrounded by a quartz sheath, and care was taken that it did not touch the outer quartz tube as shown in Fig. 2.1. In order to hang the sample a small hole was drilled at the centre of the one edge of the

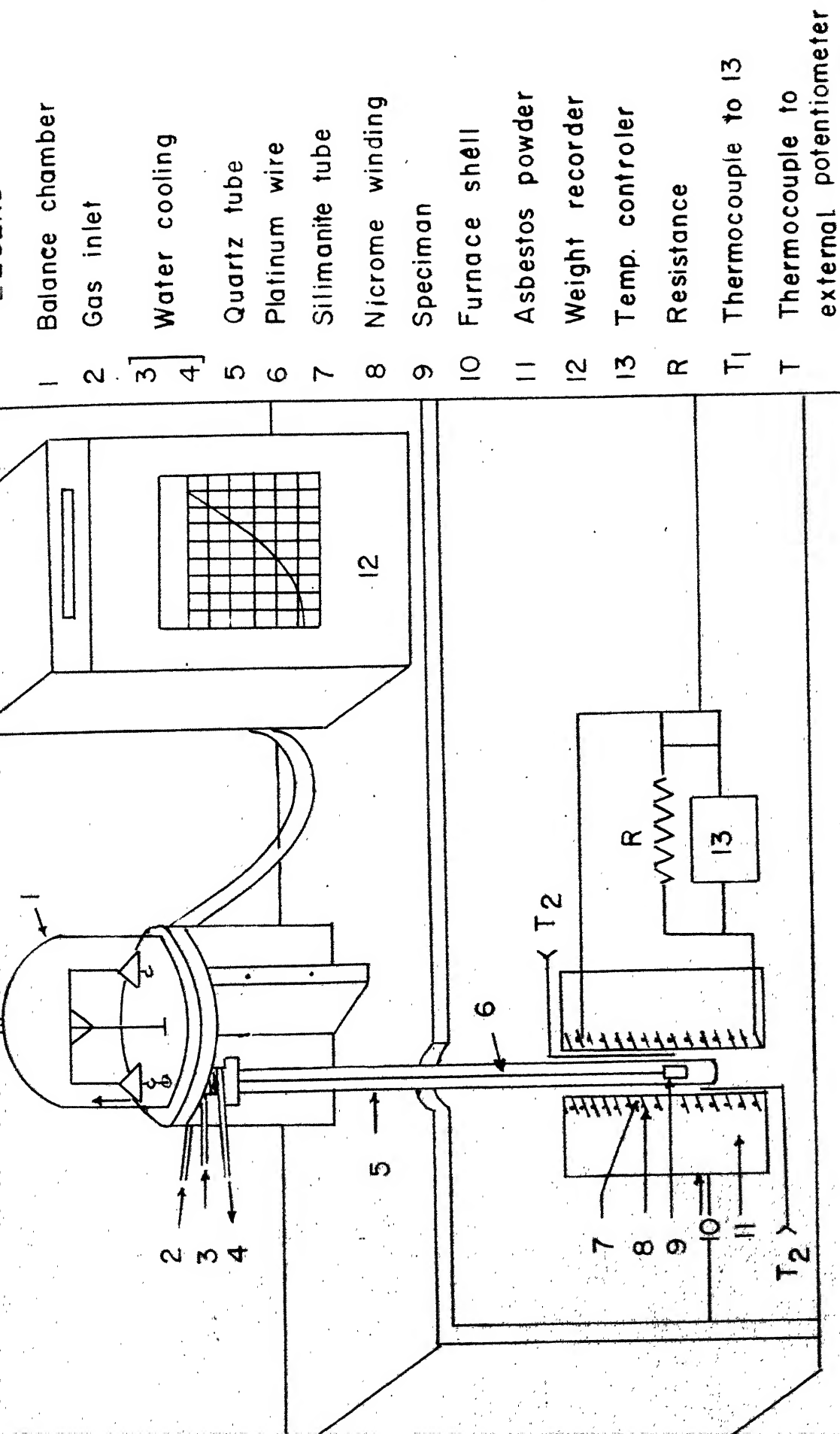


Fig.2.1 Reaction chamber and wt. recording unit.

specimen. The length of the platinum wire was so chosen that the suspended sample was always in the predetermined uniform temperature zone.

The furnace used during investigation, consisted of the winding of a 22 gauge nichrome wire upon 3.5 cm sillimanite refractory tube. The overall resistance of the winding was around 50 ohms. The temperature in the uniform zone of the furnace was controlled within $\pm 2^{\circ}\text{C}$ with the help of a temperature controller as shown in Fig. 2.1. The reaction tube consisting of a quartz tube was connected to the balance through a brass flange with O-rings.

A calibrated chromel-alumel thermocouple was used to record the temperature of the furnace. The junction of the thermocouple was kept as close as possible to the specimen in order to record its temperature as accurate as possible.

The furnace was rested on a screw-jack which could be moved up or down very smoothly when desired.

During the oxidation in oxygen environments, the system was thoroughly evacuated to a pressure approximately 10^{-3} torr, with the help of a mechanical pump. After that the oxygen gas was introduced into the system. The gas from the cylinder was first passed through a solution of sulphuric acid in order to remove moisture, followed by a

long tube containing soda-asbestos granuals (14-20 mesh). Latter was used in order to get rid of carbon dioxide which is usually present in commercial oxygen cylinders. The U-tube manometer shown in Fig. 2.2 (Schematic of gas-train) was used to observe the oxygen pressures. Since most of the runs were carried out at 1 atm pressure of oxygen, thus oxygen gas was passed into the system till the mercury in the two limbs of manometer showed equal level. Oxidation experiments were carried out at various oxygen pressures. In these experiments, the oxygen pressures were read from the difference in the levels of mercury in the two limbs of manometer. For carrying out experiment in oxygen-water vapour mixture, an additional bath (shown by No. 11 in Fig. 2.2) containing distilled water was added into the system. The gas after purification was bubbled into this bath which was maintained at constant temperature of 32°C . This gave the oxygen gas saturated with about 5 pct. water vapours. One oxidation run was carried out by bubbling oxygen gas through water maintained at 40°C . This gave a saturation of about 10 pct. water vapours.

Purification step was not required during the oxidation runs in air atmosphere.

To start the experiment, first step was to adjust the zero and check the sensitivity of the balance. This

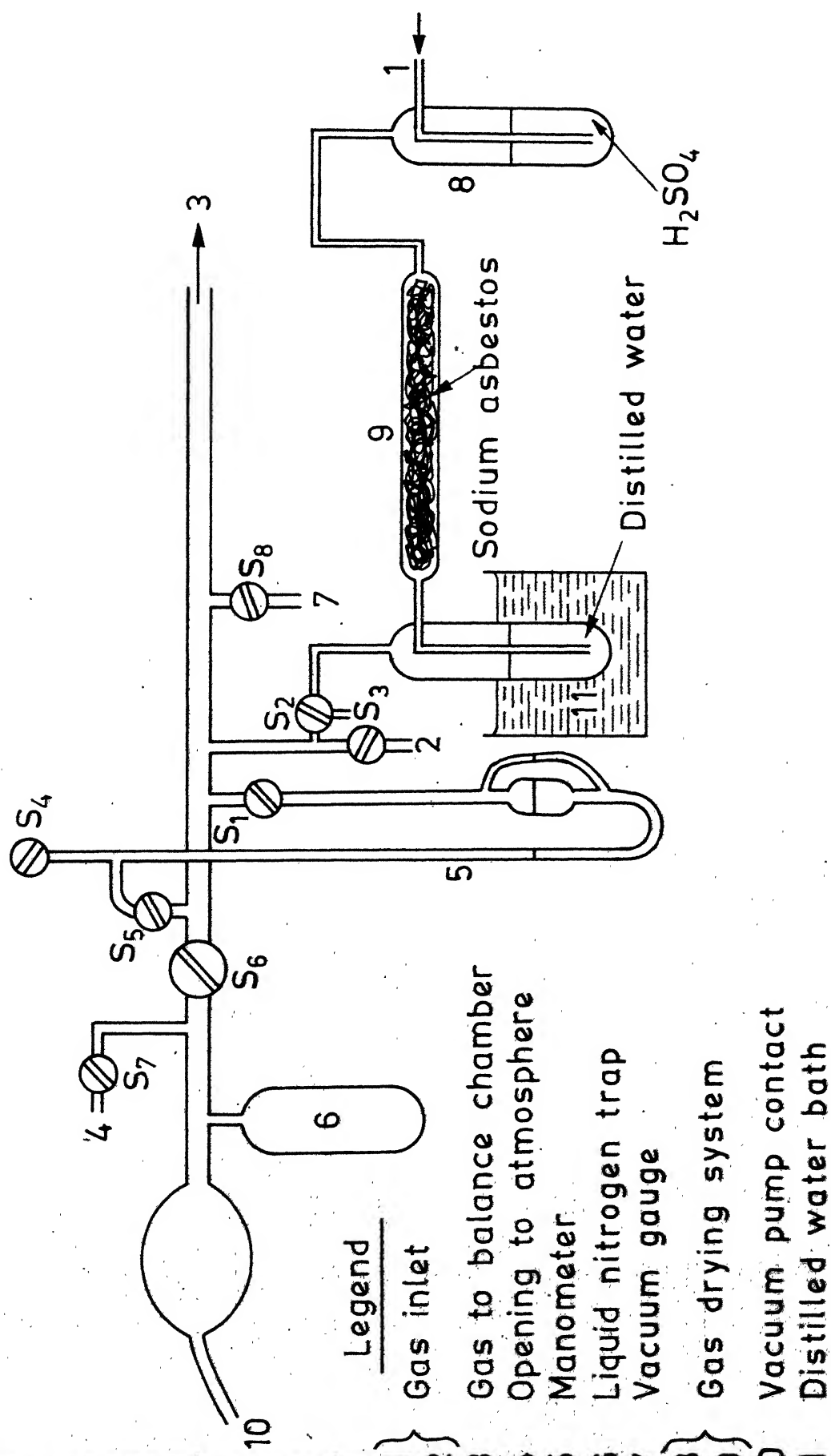


Fig. 2.2 Gas train (schematic)

was done according to the instructions provided in operating manual. It was found that the zero adjustment and sensitivity were unaffected even after 30-40 oxidation runs. Next step was to suspend the specimen on the right pan of the balance, through a hook provided on the lower side of it. Weights slightly less than the total weight of wire, quartz sheath and specimen were kept on the right pan of the balance. This difference in the weight of the two pans of the balance was adjusted by the rider weights. After the gas was passed in the system as discussed above. When the furnace reached the desired temperature, it was raised to a level by adjusting the screw jack, so as to bring the specimen in the uniform temperature zone. Once this was over, the recorder was set on to record the continuous weight gain with time.

2.5 Examination of Oxidation Products:

Oxidation runs were carried out both for very short as well as long durations. For electron microscope examinations, oxidation was carried for as short as 30 seconds duration. Most of the runs were carried out for ten hour duration. For metallography and x-ray diffraction the samples were oxidised for about twenty hour duration. Once the oxidation for a desired period was over, the furnace

was lowered and sample was allowed to cool to room temperature. Weight of the specimen was checked on a separate microbalance after its removal from the pan. The physical appearance, nature of oxide layer etc. were being noted at the same time.

Reaction products were examined by Metallography, X-ray diffraction, SEM and EDAX. Optical microscopy revealed the, oxide layer thickness, number of oxide layers and edge effect. For this, sample after oxidation was mounted in an epoxy-resin in such a way that the cross-section of the specimen could be exposed. This was then polished up to velvet cloth where suspension of alumina particles were used as abrasives. Thus cross-section of the specimen was observed.

Scanning electron microscope pictures were taken for air oxidised specimens. With the help of this, it was possible to differentiate the various oxide layers, which was not possible in optical microscopy.

Concentration profiles for the constituent elements were determined throughout the oxide layer using EDAX. Only air oxidised samples were used for this purpose.

To determine the composition of oxide layer, X-ray analyses were carried out. X-ray diffraction runs were carried out using copper target. The oxide layers were

stripped off either mechanically or by chemical dissolution technique. These layers were crushed to powder form and mounted in a specimen holder made of pyrex. X-ray diffraction runs of some known oxides were also taken. Thus by matching the peak intensities, the oxides were identified.

A few specimens, which were oxidised for a very short duration, so that the oxide layer was thin enough to transmit the electrons, were studied using electron microscope. The oxide layer was stripped off using dissolution technique, and was seen in microscope. Both surface topography and electron diffraction pictures were taken.

CHAPTER 3

THERMOGRAVIMETRY

Thermogravimetry is a technique whereby a sample is continuously weighed as it is heated at a constant rate. The resulting weight gain vs temperature curve can provide three basic areas of quantitative information, (1) change in composition, (2) range of thermal stability and (3) evaluation of kinetic parameters. Present work emphasises the utility of last one.

The application of TGA to the determination of process kinetics is of extremely valuable, since from one dynamic temperature experiment one can often derive data which would require a much longer period of time under isothermal conditions. At any temperature (or time) on the TGA thermogram both sample weight and the rate of weight loss are available from the record, thus providing all the information required for kinetic calculations. In present work however, such approach is not employed. Isothermal runs were taken at various temperatures using a thermobalance in order to determine process kinetics. However, one such dynamic temperature experiment was carried out on powdered steel sample, on a derivatograph. Simultaneous TGA and DTA plots obtained are shown in Fig. 3.1. Heating rate was 10° per minute.

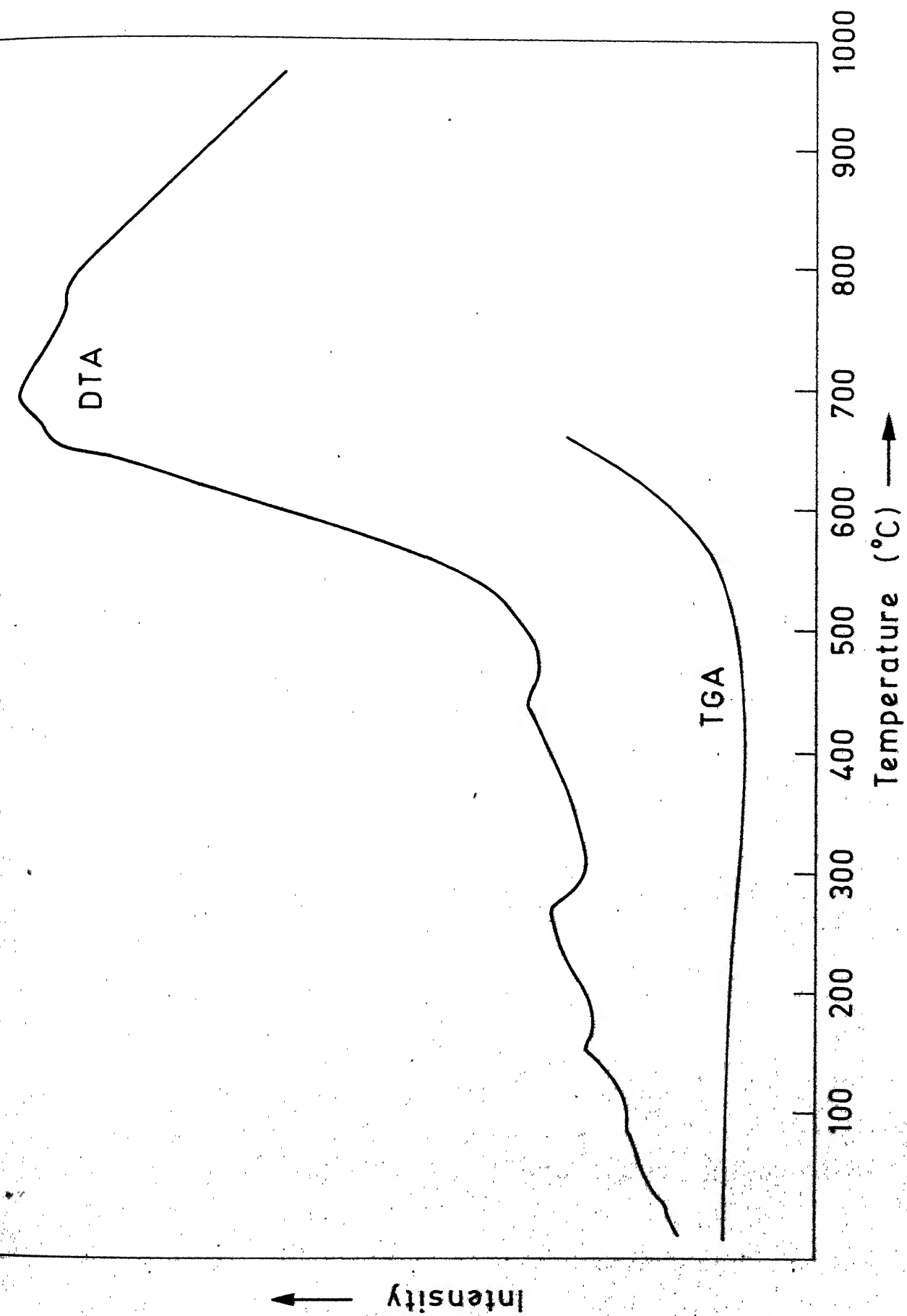


Fig. 3.1 Simultaneous TGA and DTA curves.

and experiment was carried out from room temperature to 1000°C . Upper curve shown in fig. is for DTA and lower one for TGA. Since the reaction was carried out in air, thus only reaction possible was oxidation. It is clear from the TG curve that, there is no oxidation below 500°C and above this weight gain increases tremendously. Since, almost all weight change processes absorb or release energy and are thus measurable by DTA. The corresponding peak in DTA curve, where weight gain occurs in TG curve, indicates the formation of an oxide. Few small humps below 500°C may be due to some tarnishing etc. on the surface of alloy.

Isothermal runs were carried out in air, dry oxygen, oxygen-water vapour mixture from a temperature 500°C to 1000°C . Description of the samples employed in this investigation is given in tables 1 to 4 in Appendix-1. The samples have been classified in four categories, based on the type of environment used. Those oxidised in air were designated by numbers, 1,2,3...etc., those oxidised in oxygen were designated by Roman numerals, I, II, III etc. and those oxidised in oxygen water vapour mixture were designated as W_1 , W_2 ... etc. Table 3A gives the details of specimens which were oxidised at various oxygen pressures and were

designated by P_1 , P_2 ... etc. These tables summarize the basic information about specimens i.e. surface area, thickness, temperature of oxidation, duration, final weight gain in mg/mm^2 and physical appearance of sample after oxidation.

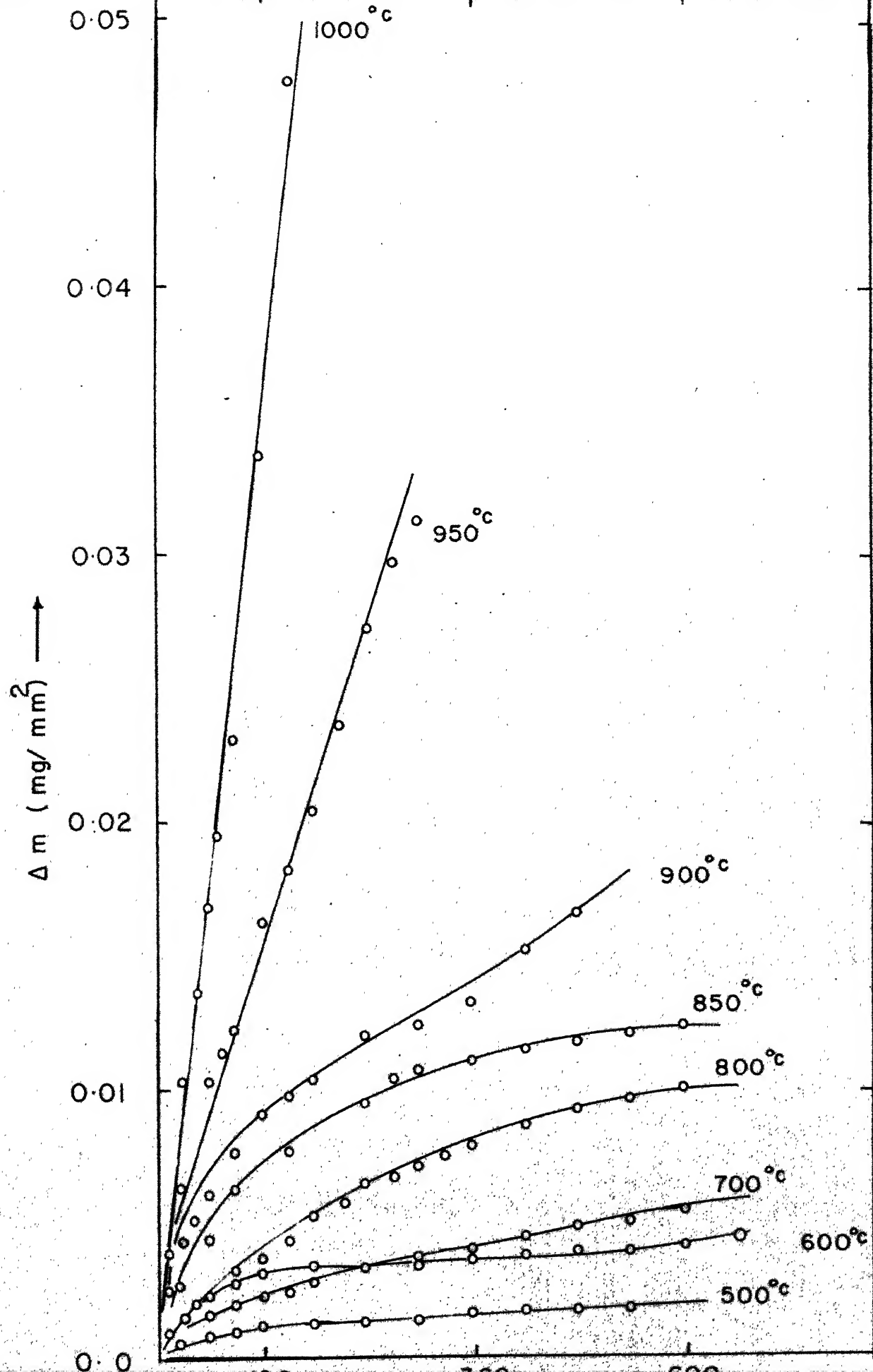
Thermogravimetric data for the various samples have been given in tables 5 to 8 in Appendix 1. These data have been plotted in Fig. 3.2 to 3.4 as graphs of weight increase as a function of time. It is very difficult to gether information about oxidation laws from these linear plots. Thus in order to know the oxidation laws, one starts with a very general equation:

$$(\Delta W)^n = kt$$

where ΔW is the weight gain with time t , n is known as the power index which tells about the particular rate law and k is the rate constant. If $n=1$, rate is linear, if $n = 2$, it is parabolic and so on. Above equation can be written after taking logs on both side in following manner:

$$n \ln \Delta W = \ln t + \ln k$$

Thus a linear plot of $\ln \Delta W$ vs $\ln t$ can give a straight line, the slope of which will give the value n . Figs. 3.5 to 3.7 show such plots for oxidation in air, oxygen and oxygen-water vapour mixture. The information obtained from these curves is summarized in tables 3.1 to 3.3.



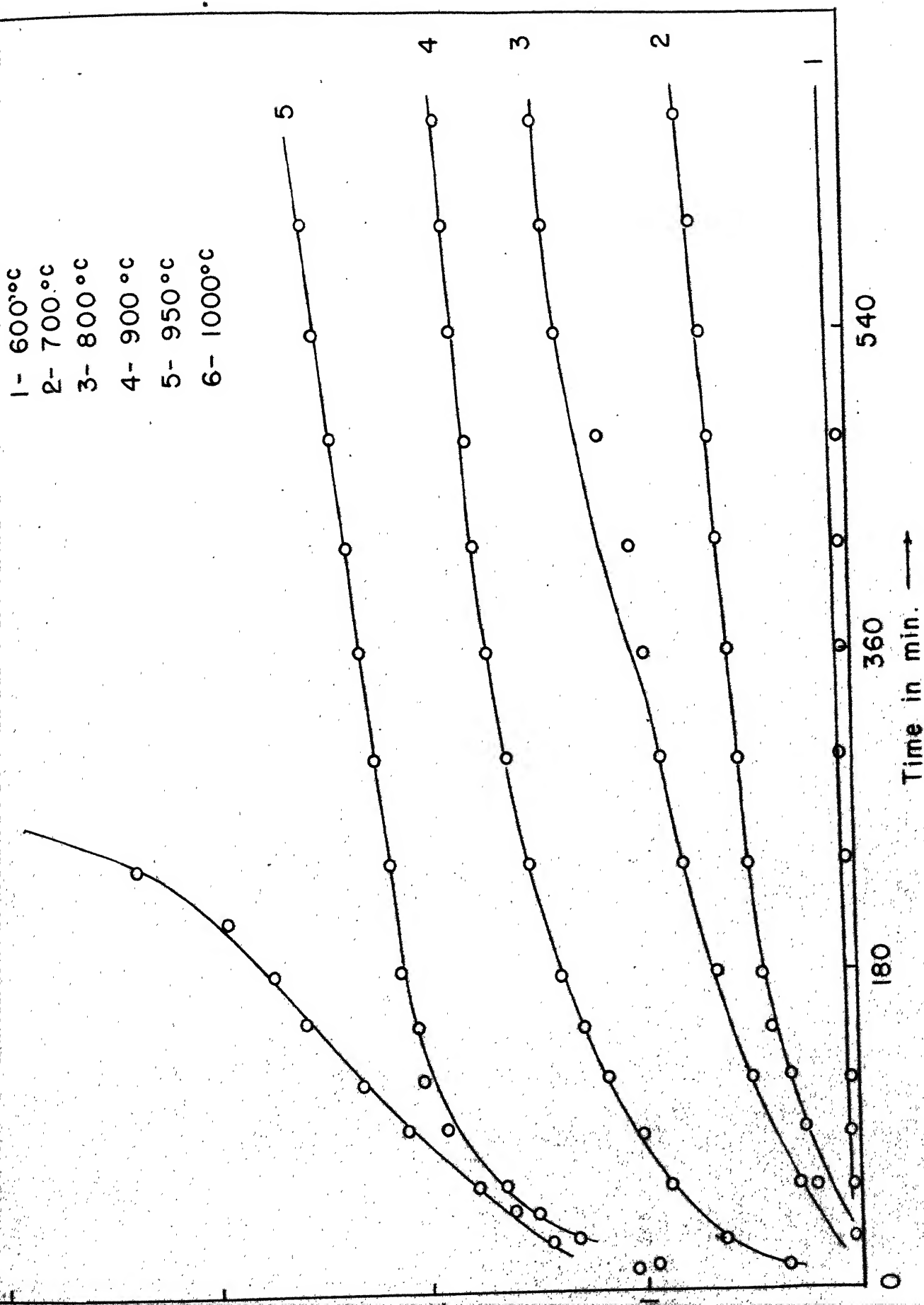
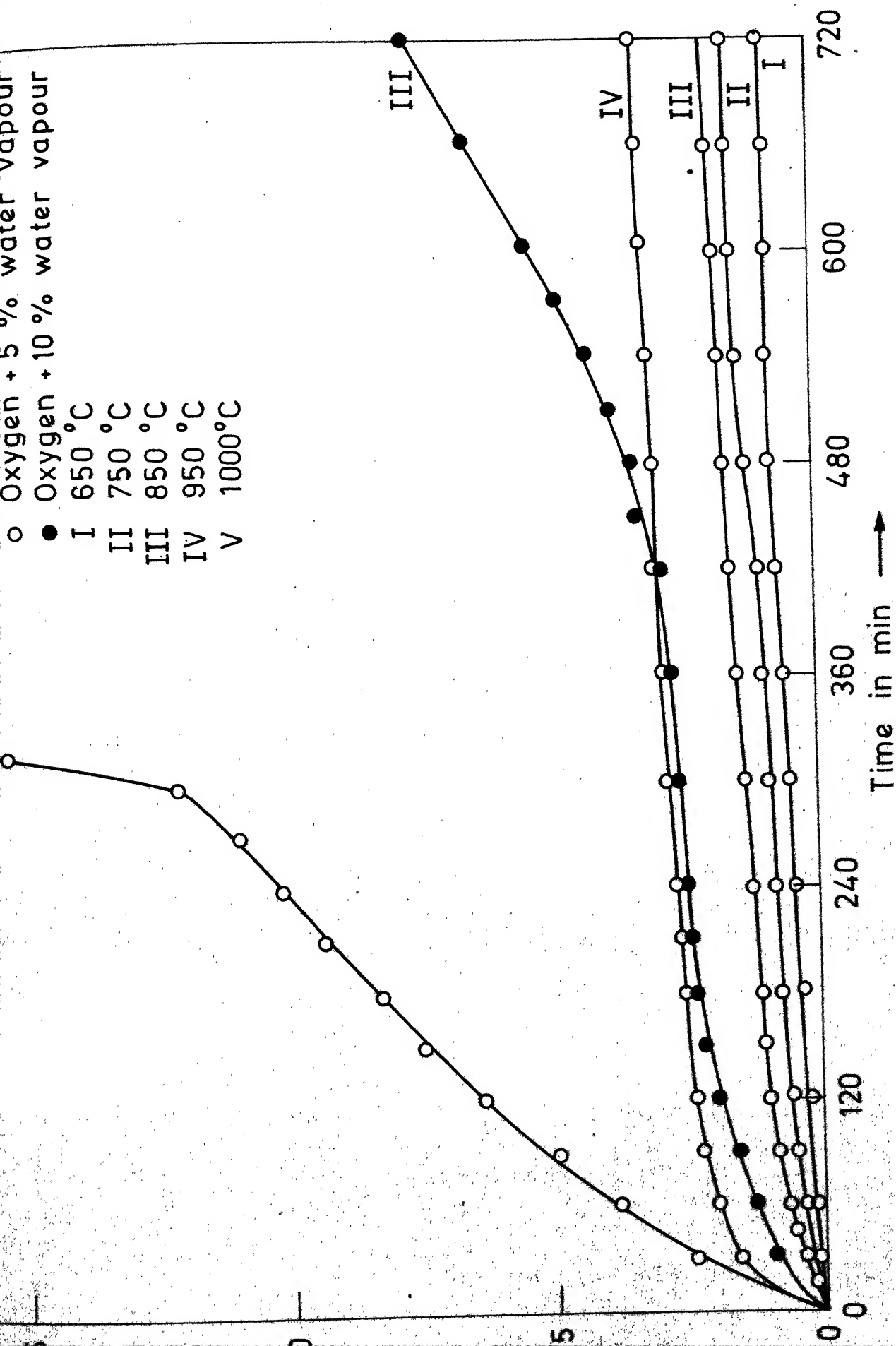


FIG. 2.3. Linear plot for the oxidation of 2.5 Cr-1 Mo steel in dry oxygen



3.4 Weight gain vs time plot of 2.5 Cr-1 Mo steel in oxygen-water vapour mixture at various temperatures

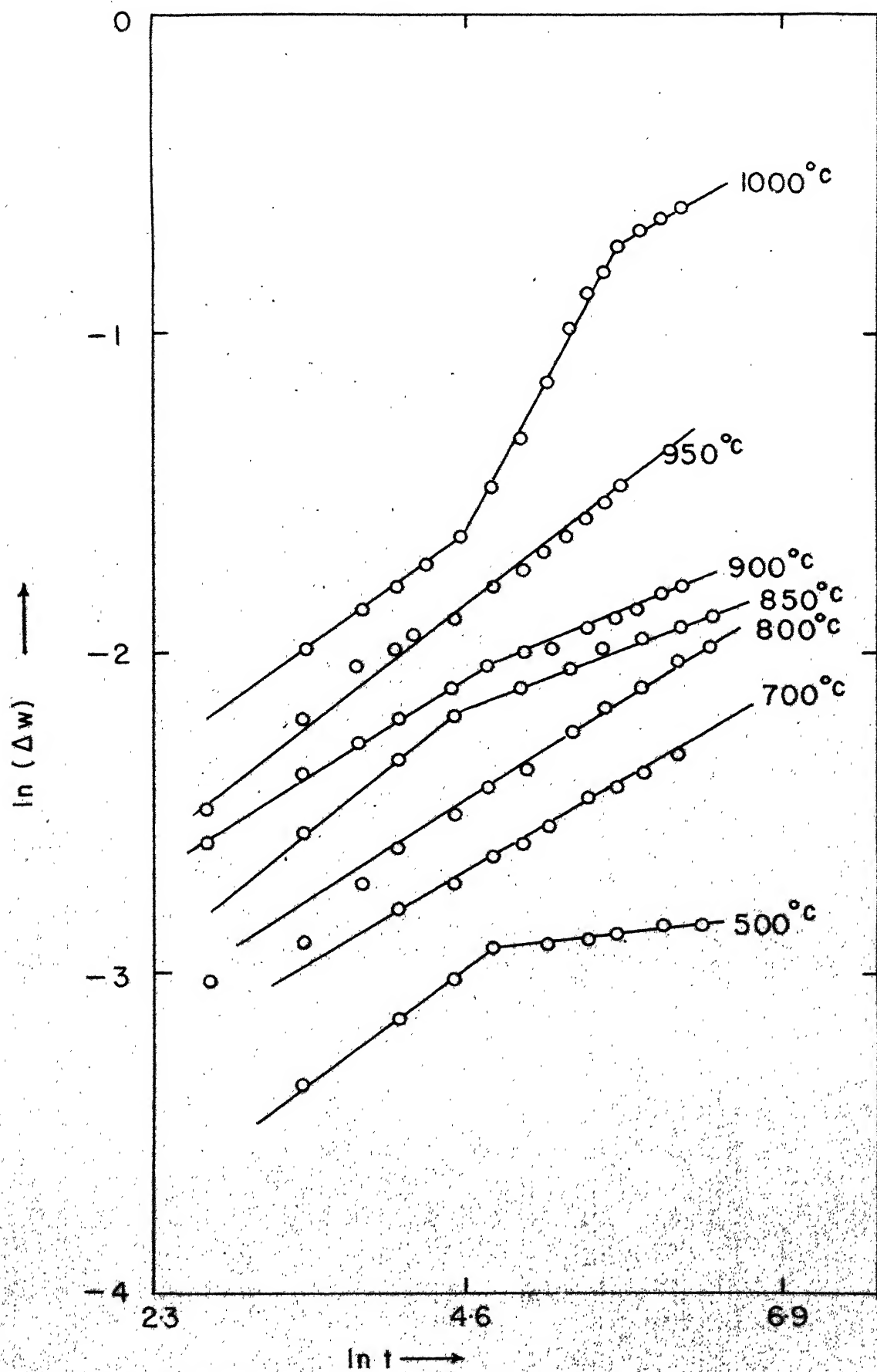


Fig. 7. Double-log plot of $\ln \Delta w$ vs. time of 25 Cr-1 Mn alloy.

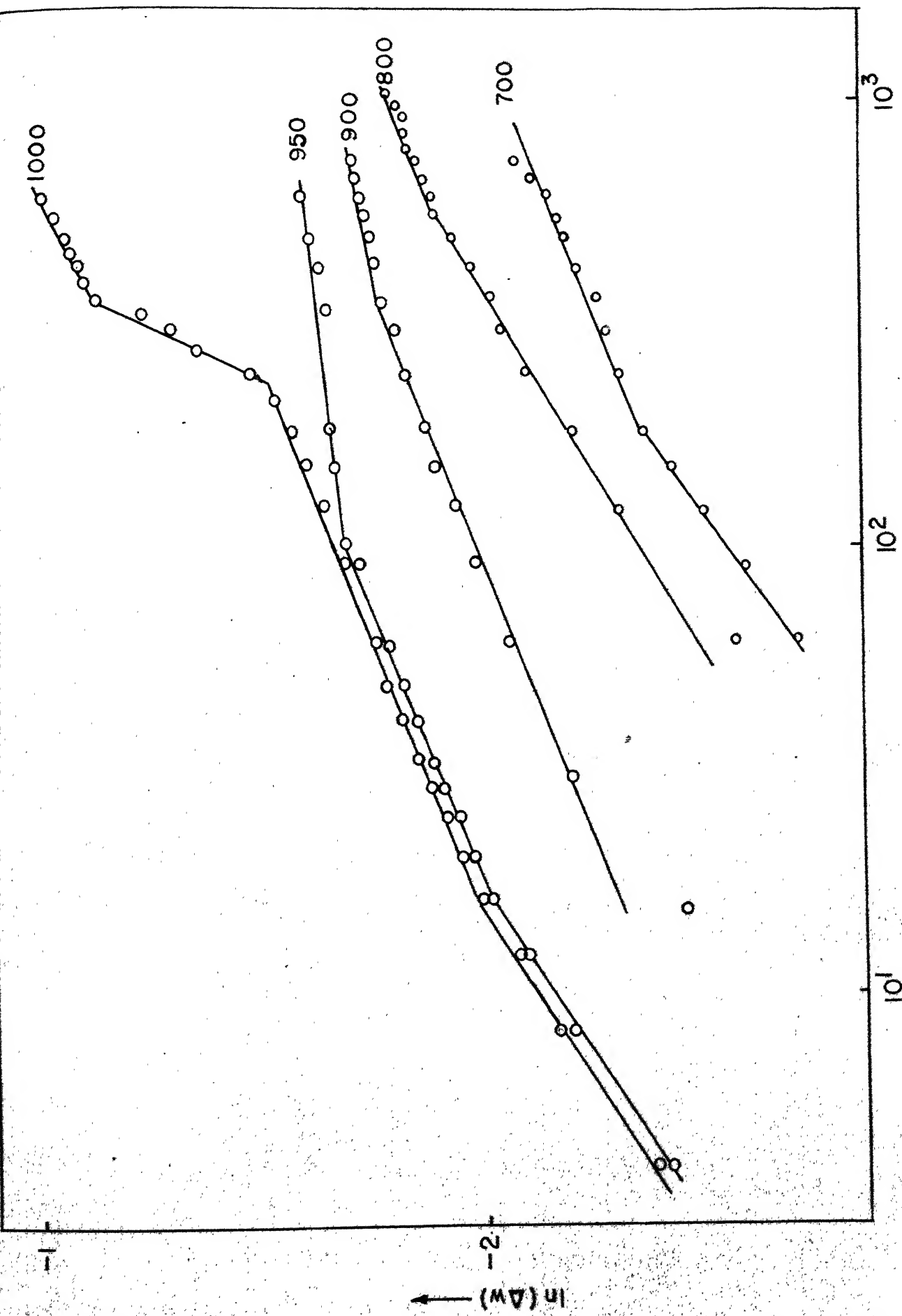


Figure 1. Plot of $\ln \Delta w$ versus $\ln t$ for the oxidation of 2.5 Cr-Mo steel in dry

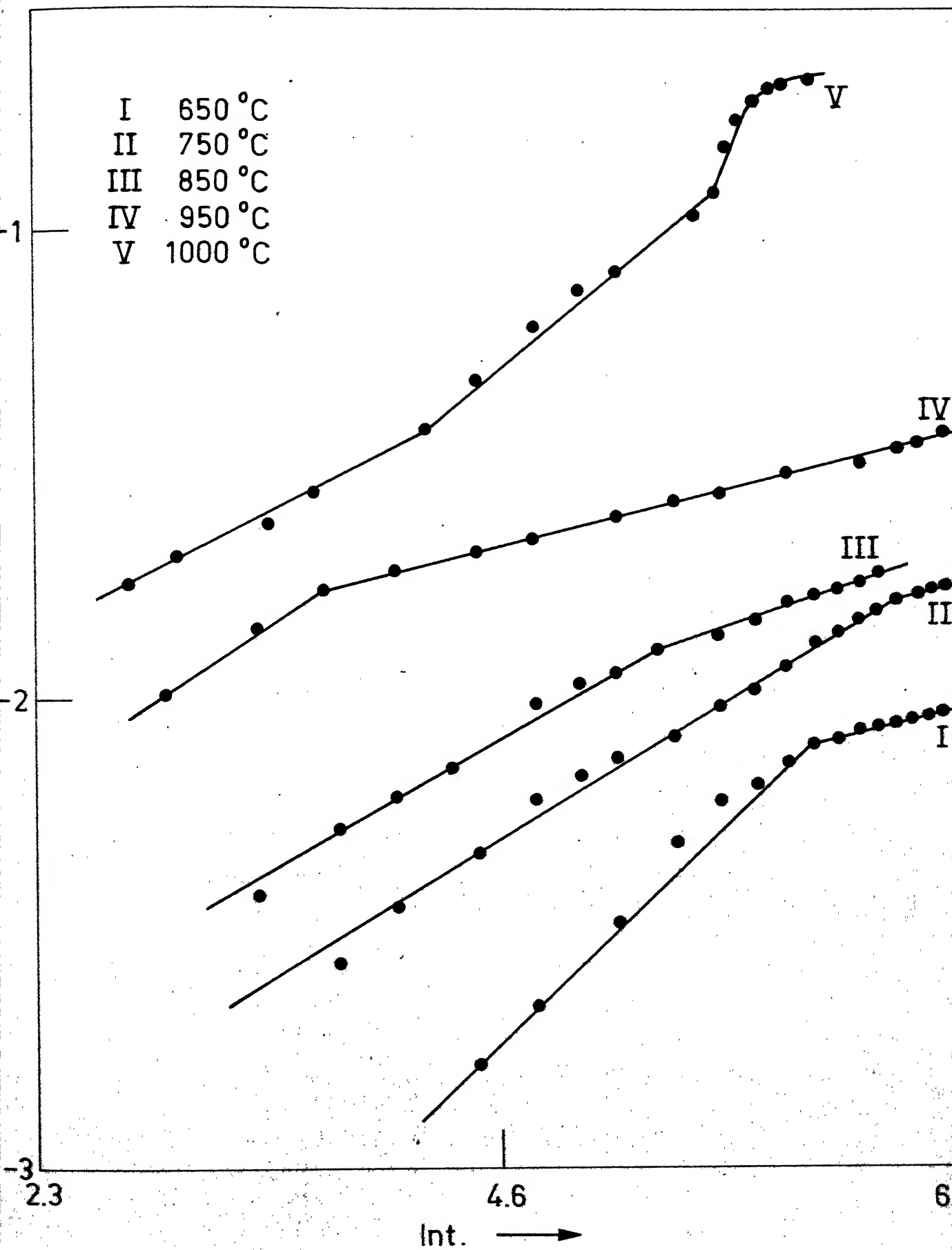


Fig. 3.7 Double log plot of weight gain vs time of 2.5 Cr -

Table 3.1

Variation of m and k according to equation

$$(\Delta W)^n = kt \text{ for air oxidation}$$

Temperature of oxidation °C	Time interval for which 'n' holds	Value of 'n'	Value of rate constant	
500	0-100 min	1.4	$4.8 \times 10^{-4} \text{ mg mm}^{-2} \text{ min}^{-1}$	log
	100 min			
600	100 "	(log)	$1.0 \times 10^{-3} "$	Parabolic
700	30 "	1.7	$3.5 \times 10^{-8} \text{ mg}^2 \text{ mm}^{-4} \text{ min}^{-1}$	
800	30 "	1.6	$2.5 \times 10^{-7} "$	
850	0-60 "	1.17	-	cubic
	60 "	2.7	-	
900	0-90 "	1.5	-	linear
	90 "	3	-	
950	Throughout	1.3	$8.66 \times 10^{-5} \text{ mg mm}^{-2} \text{ min}^{-1}$	
1000	0-100 min	1.3	$2.9 \times 10^{-4} "$	
	100-300 "	1.5		
	300 "	2		

Table 3.2

Variation of n and k according to equation

$$(\Delta W)^n = kt \text{ for oxidation in oxygen}$$

Temperature of oxidation °C	Time interval for which 'n' holds	Value of n	Value of parabolic rate constant $\text{mg}^2 \text{ mm}^{-4} \text{ min}^{-1}$
700	0-180 min	1.5	9.96×10^{-8}
	180 "	2.75	
800	0-650 "	1.78	2.9×10^{-7}
	650 "	3	
900	0-350 "	2.3	8.1×10^{-7}
	350 "	7	
950	0-20	1.7	2.3×10^{-5}
	20-100	2.35	
1000	0-20	1.7	6.5×10^{-5}
	20-240	2.4	
	240-360	0.5	
	360	2.0	

Table 3.3

Variation of n and k according to equation

$$(\Delta W)^n = kt \text{ for oxidation in oxygen water}$$

vapour mixture

Tempera- ture of oxidation, °C	Time interval for which 'n' holds	Value of 'n'	Value of parabolic rate constant (mg ² mm ⁻⁴ min ⁻¹)
650	0-45 min	1.1	1.3x10 ⁻⁷
		5	
750	0-700 ''	1.75	
	700 ''		3.5x10 ⁻⁷
850	0-240	1.9	6.1x10 ⁻⁷
	2.8 ''	2.8	
950	0-40 ''	1.5	
	40 ''		4.78 x 10 ⁻⁶
1000	0-70 ''	1.95	
	70-300 ''	1.3	17.0 x 10 ⁻⁶
	300-360	.5	
	360	2	

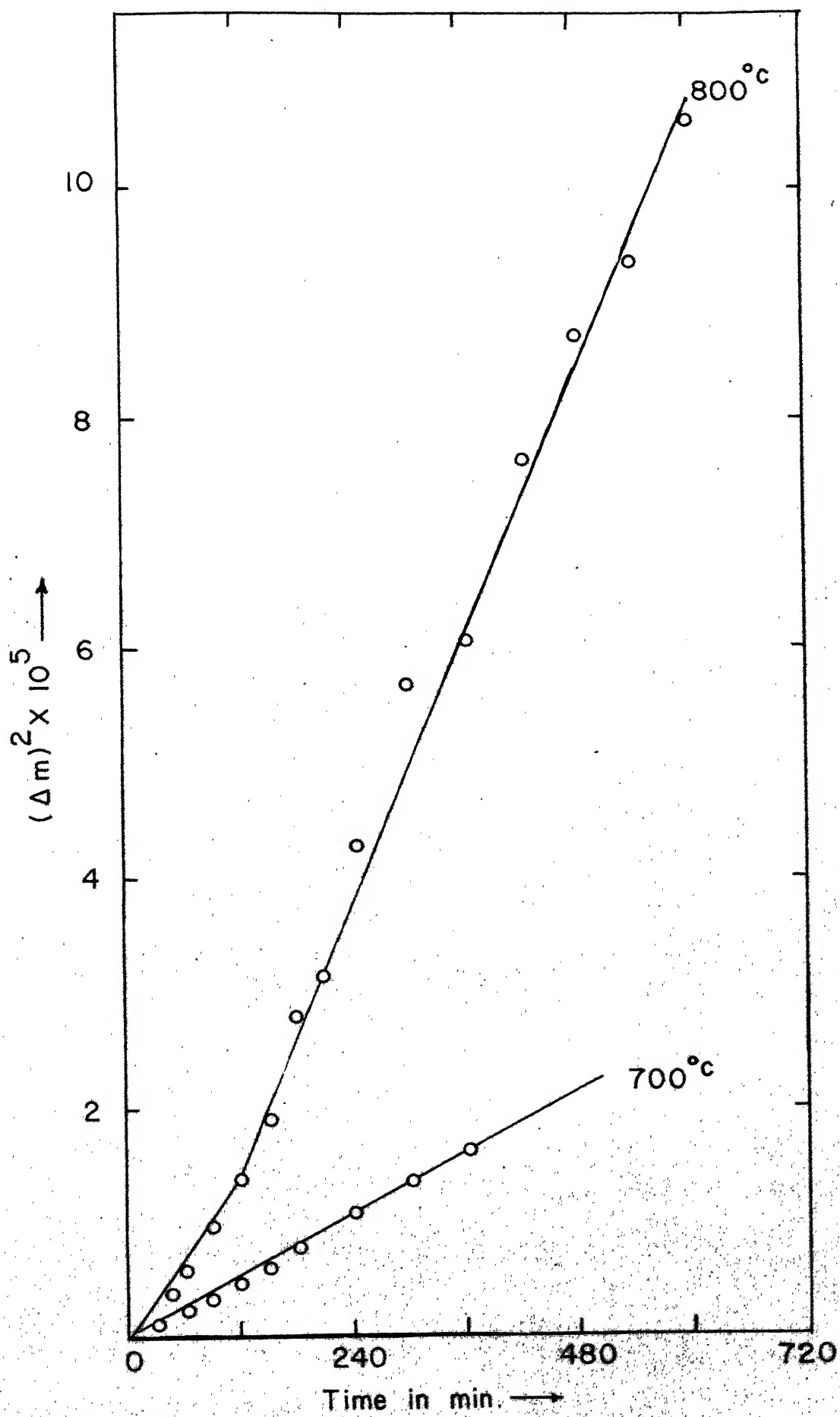
Double logarithmic plots may accordingly appear to be convenient method of evaluating 'n', which has values of 1,2,3 for linear, parabolic and cubic oxidation respectively. However, the scale in such plots becomes increasingly compressed with increasing value of (ΔW) and t . For this reason such plots tend to suggest linear relationship between $\ln (\Delta W)$ and $\ln t$, and changes in rate equations and mechanisms are not easily identified. For confirming the rate laws, proper rate equation must be recognised. Thus if the information obtained from double log plots, suggests that the rate is parabolic it must be confirmed by plotting $(\Delta W)^2$ vs time plots. Fig. 3.8 and 3.9 show such plots for oxidation in air and, oxygen and oxygen-water vapour mixture. These figures clearly show that rate follows parabolic behaviour up to the time indicated by double log plots, after that some other rate law takes over. Similarly Fig. 3.10 indicates W vs $\ln t$ curve showing that oxidation law is logarithmic upto 650°C in air and oxygen.

3.1 Effect of Temperature and Time:

3.1.1 Oxidation in air: In air the oxidation is very small at low temperatures. As indicated in table 3.1, initial oxidation upto 600°C is linear for about 100 min and becomes

CENTRAL LIBRARY

Acc. No. A 62326



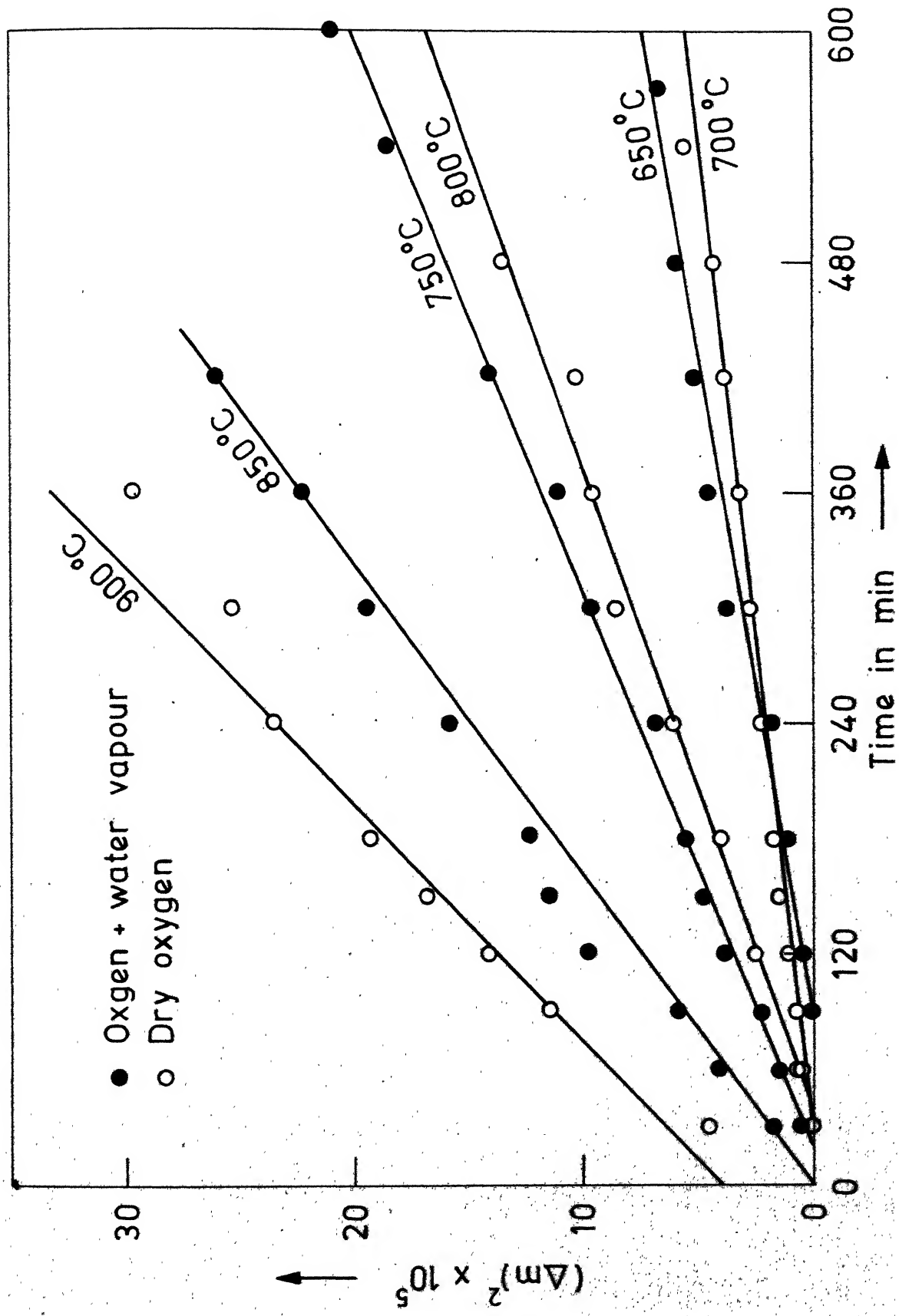


Fig. 3.9 Square of the weight gain vs time plot of 2.5 Cr - 1 Mo steel in O_2 and $O_2 + H_2O$ vapour.

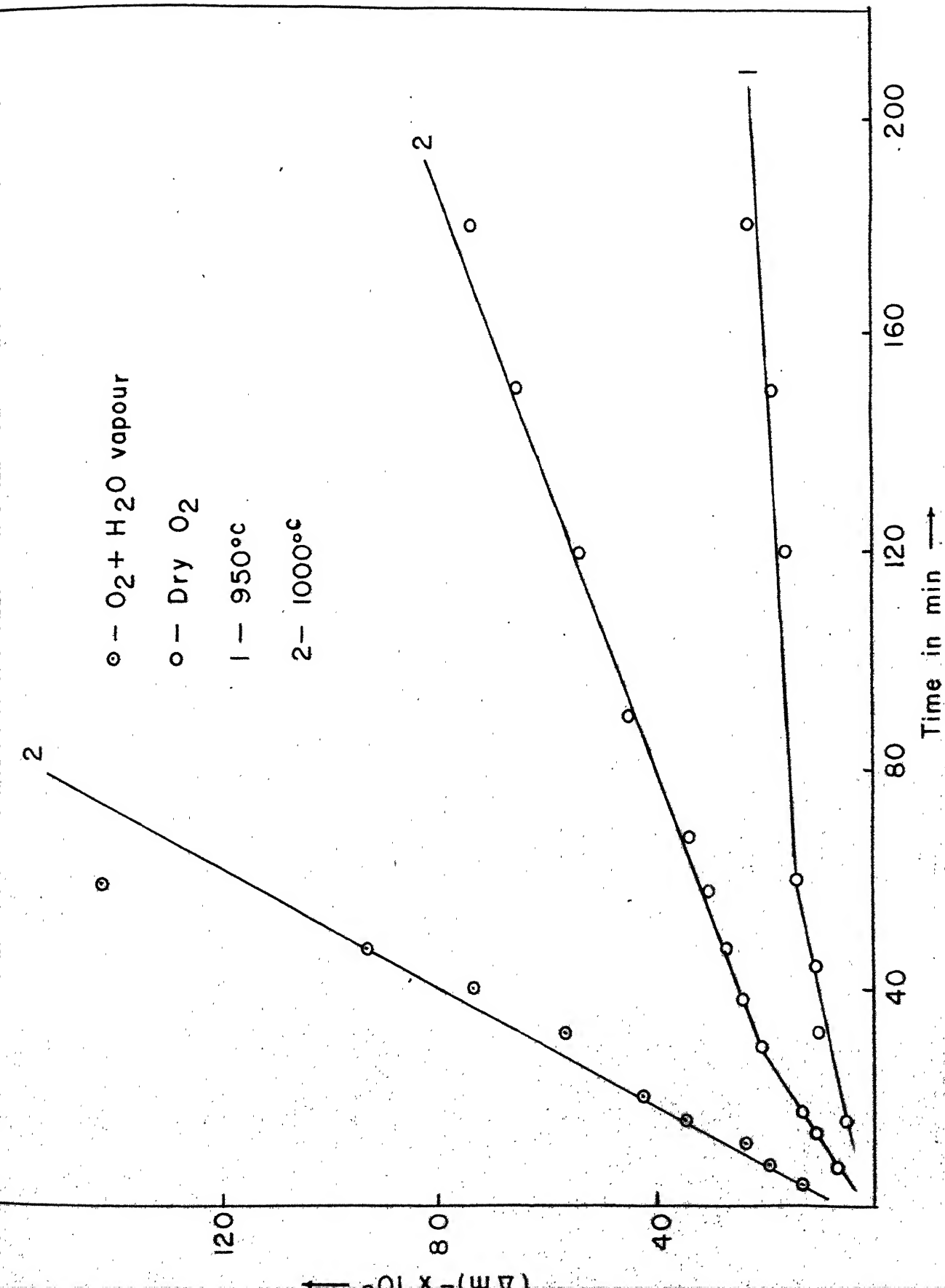


FIG. 3.9A— Square of wt. gain vs. time plot of 950°C and 1000°C

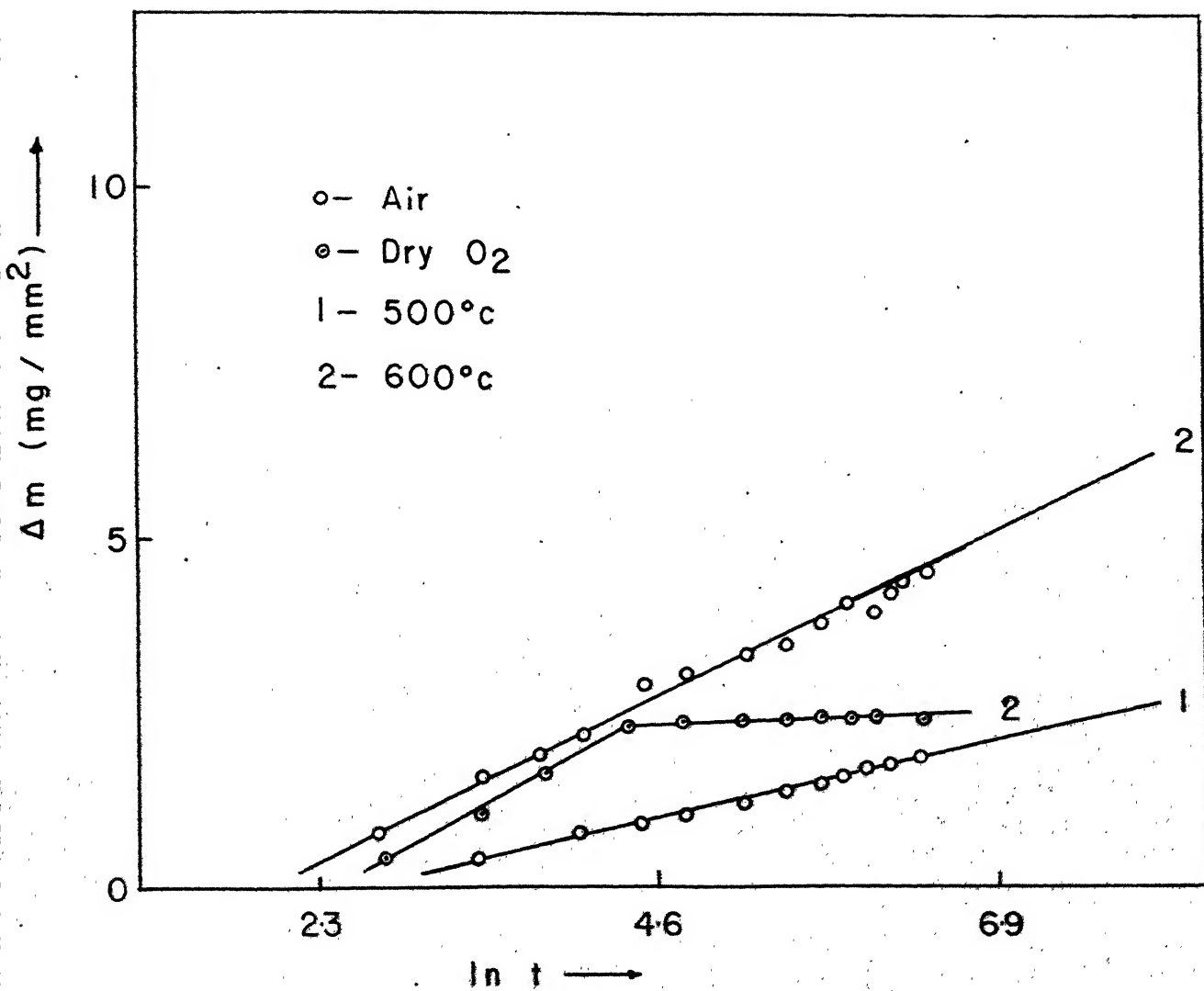


FIG. 3-10 $\ln t$ vs Δm plot for 2.5Cr-1Mo steel in air and oxygen

logarithmic afterwards. At 700°C and 800°C true parabolic behaviour is shown which is further confirmed by the $(\Delta W)^2$ vs t plot. A break at very small time can be explained by the fact that rates are not generally parabolic near zero time. At 850° and 900°C , rate is linear for an initial small period and then becomes cubic. Linear kinetics are observed above this temperature.

3.1.2 Oxidation in dry oxygen

Upto 600°C rate is found to follow logarithmic behaviour. Above this temperature there seems to be a combination of more than one rate law. At all temperatures above 600°C , oxidation starts initially parabolically, then changes mechanism after certain time. This time is large at low temperatures and small at high temperatures. On comparison of rate constants as given in table 3.2, it is clear that the rate of oxidation is about ten times at 900°C and hundred times at 1000°C , than the oxidation at 700°C . At 1000°C , after an initial parabolic oxidation rate, a sudden increase in weight was observed and again the oxidation was found to follow parabolic behaviour i.e. break away type of oxidation was observed.

3.1.3 Oxidation in oxygen water vapour mixture

Oxidation is parabolic at all temperatures in the beginning, but changes over to some other rate law after some time. Rate of oxidation is faster at high temperatures. On observing the rate constants given in table 3.3, it can be seen that the rate of oxidation at 850°C is about four times faster than at 650°C and that at 1000°C , it is about 100 times faster than at 650°C . At 1000°C , a similar behaviour as found in case of dry oxygen was observed.

3.2 Effect of Surface Finish:

Since oxidation is essentially a surface phenomena, the surface finish of the specimen may affect the oxidation rate. Since large number of specimens were used in the tests, specimens polished upto 4/0 finish using emery paper were used throughout the experiments. In order to observe the effect of surface finish on oxidation rate in air, some of specimens were polished up to different surface finish. Details about the sample preparation is given in table 2 in the Appendix-1. Fig. 3.11 gives the plot of weight gain vs time for these samples. The results indicate that the oxidation rate is more for a rough surface than for a fine one. An electropolished surface had the lowest

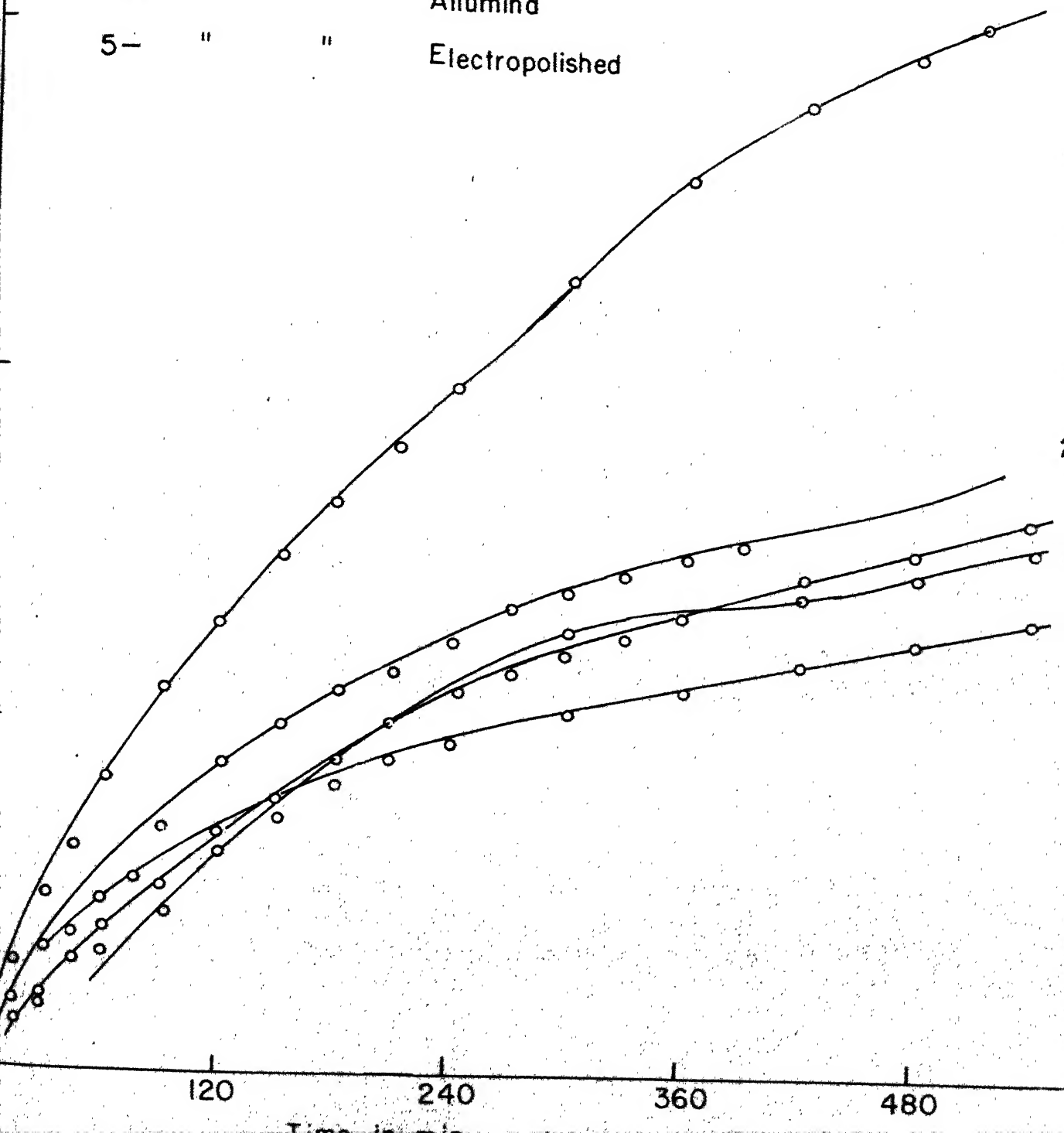
1- Rough polished on belt

2- Polished up to 1/0 emery paper

3- " " 4/0 " "

4- " " Allumina

5- " " Electropolished



rate which is quite obvious as it provides a stable (stress free) surface. The results are in agreement with that reported by various workers^(1,2,3).

3.3 Effect of cold work on oxidation rate:

While preparing samples for oxidation tests, by abrading, lot of cold work is introduced. In order to observe the effect of this, on oxidation rate, some of the cold rolled strips (discussed in chapter 2) were first annealed at 850°C and then the samples were cut and polished upto 4/0 emery finish and used for oxidation. These samples were termed as cold worked samples and their oxidation rate was compared with the annealed specimens. The oxidation was carried out for these two types of specimens in air at temperatures 650°C , 750°C , 850°C and 950°C . Results obtained are indicated in table 3.4. In this table, weight gain measured for cold-worked specimen is compared with that of an annealed one. It indicates that at 650°C where logarithmic law is followed for oxidation the weight gain is more for, ^{an}unannealed one. Also there is no significant change for the weight gain for 750°C where oxidation follows parabolic behaviour. These results are in agreement with the reported results by Uhlig⁴. According to him factors

Sample No		Temp. of Oxidation	Total wt. gain mg/mm^2		Nature phy. appearance of oxide layer	
Annl.	Un-annealed		Annealed	Un-annealed	Annealed	Un-annealed
65	55	650°C	5.84×10^{-3}	7.36×10^{-3}	Dark grey coloured non-adherent (more than un-annealed) oxide layer	Dark gray coloured highly non-adherent (loose) oxide layer
64	56	750°C	2.17×10^{-2}	2.10×10^{-2}	Dark grey coloured adherent, very uniform, smooth oxide layer	Same – except the degree of uniformity and smoothness is less
66	57	850°C	122	275	Grey coloured uniform oxide layer	Same – except the smoothness and uniformity is less
63	58	950°C	369	392	Dark black coloured thick non-uniform oxide layer with white patches	Same as in annealed sample

x Duration of the oxidation was 18 hrs. in all the tests

like heat treatment and cold working are not important when oxidation is controlled by diffusion of reactants from the environment and are most important, when reactions occur at metal surface. It is well known that parabolic law is diffusion controlled while in logarithmic behaviour reaction occurs at the surface. The decrease in weight gain for cubic law as indicated in table 3.4 for 850°C cannot be explained by above argument. But according to Kofstad⁵ a cubic law is combination of parabolic and logarithmic law, thus according to Uhlig's⁽⁴⁾ argument, slight increase of rate at 850°C is justified. At 950°C a small change in weight gain of the annealed sample over the unannealed one, can not be explained, due to lack of our knowledge about the processes occurring during linear range.

3.4 Effect of oxygen pressure:

Rates of oxidation of metals and alloys may exhibit varying oxygen pressure dependence according to the rate-determining mechanism. Present work demonstrates the oxygen pressure dependence of 2.5 Cr - 1 Mo steel carried out at 800°C . Oxygen pressure as low as 240 mm Hg was tried. Details are given in table 3A in Appendix-1. The weight gain vs time plots are shown in Fig. 3.12, which shows clearly that as the pressure decreases the oxidation rate

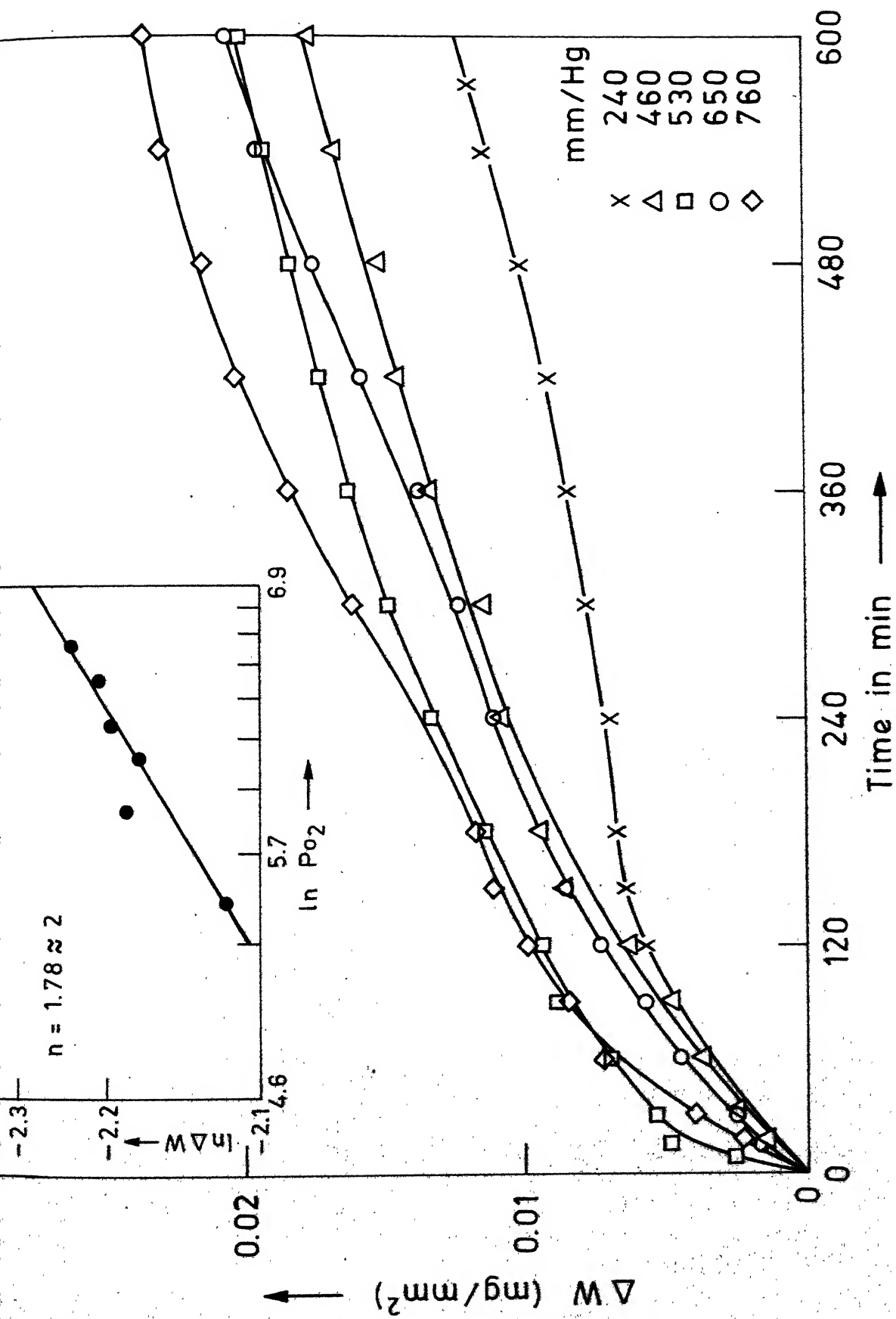


Fig. 3.12 Weight gain vs time plot of 2.5 Cr - 1 Mo steel at different oxygen pressure.

decreases. For parabolic oxidation, according to wagner, the oxygen pressure dependence can be expressed as $P_{O_2}^{1/n}$ for p-conducting scales, where n is determined by the charge on the migrating defects, while growth of n-conducting scales is independent of pressure. Thus a plot of $\ln \Delta W$ vs $\ln P_{O_2}$, shown on the left corner of the same graph, gives a value of $n \approx 2$ which means that the scale may be p-conducting and the migrating species having a charge of 2. Thus the possibility of a p-conducting scale cannot be ruled out at this temperature.

3.5 Reproducibility of thermogravimetric results:

Almost all the runs were carried out in duplicates. It was observed that each run was fairly reproducible in the initial stages. The two curves used to overlap in the beginning, but as considerable time elapsed, some separation was observed. There was about 5 to 10 pct. deviation in final weight gain in few samples. This is illustrated by an oxidation run at 1000°C in oxygen. Weight gain curves for both the samples are shown in Fig. 3.14 by 1a and 1b. In the initial stages, both the curves are overlapping but the gap between the two widens as the oxidation proceeds for longer times. But in both cases, the sudden weight gain i.e. breakaway point is same that is at 352 seconds. This

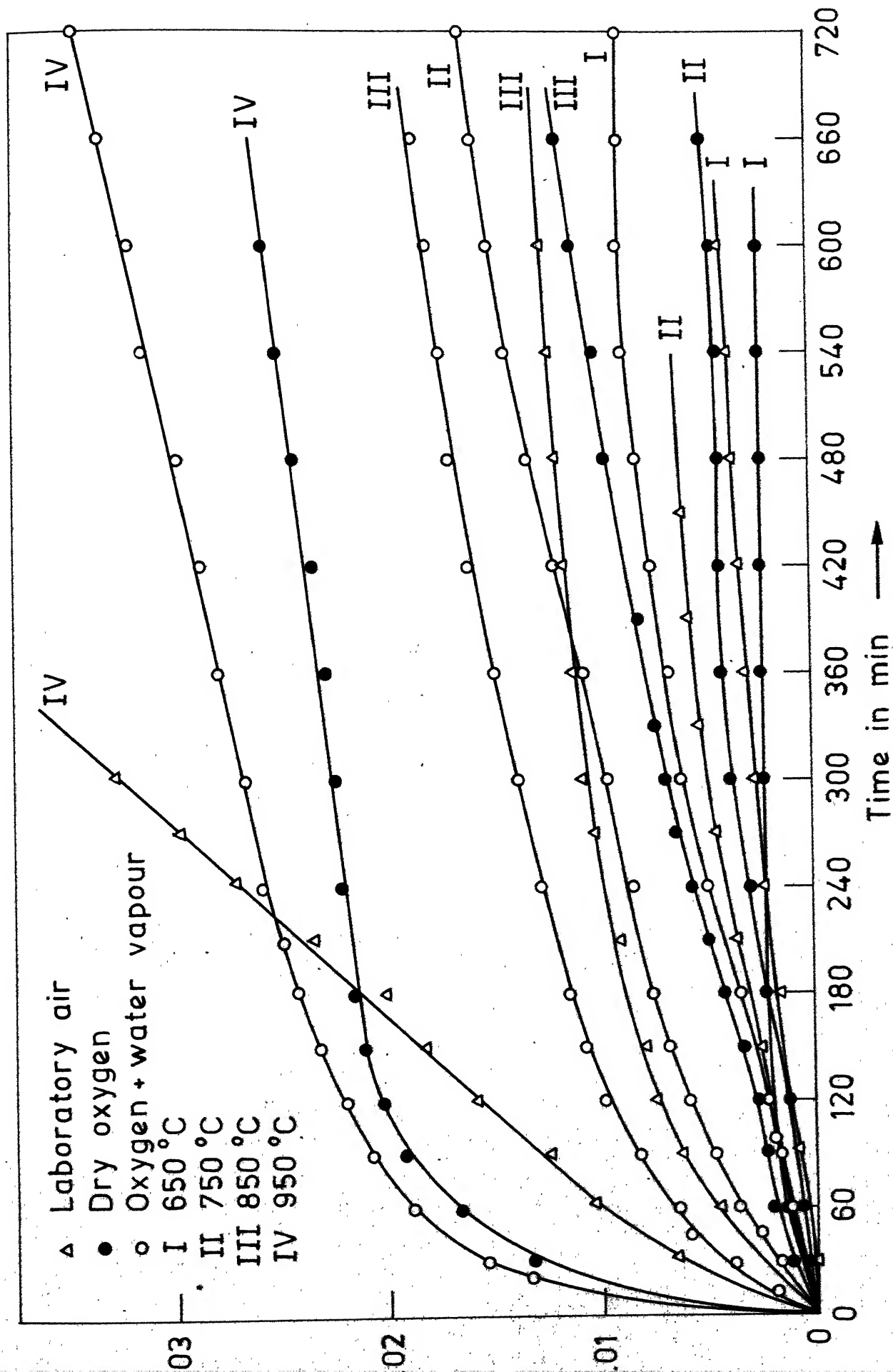
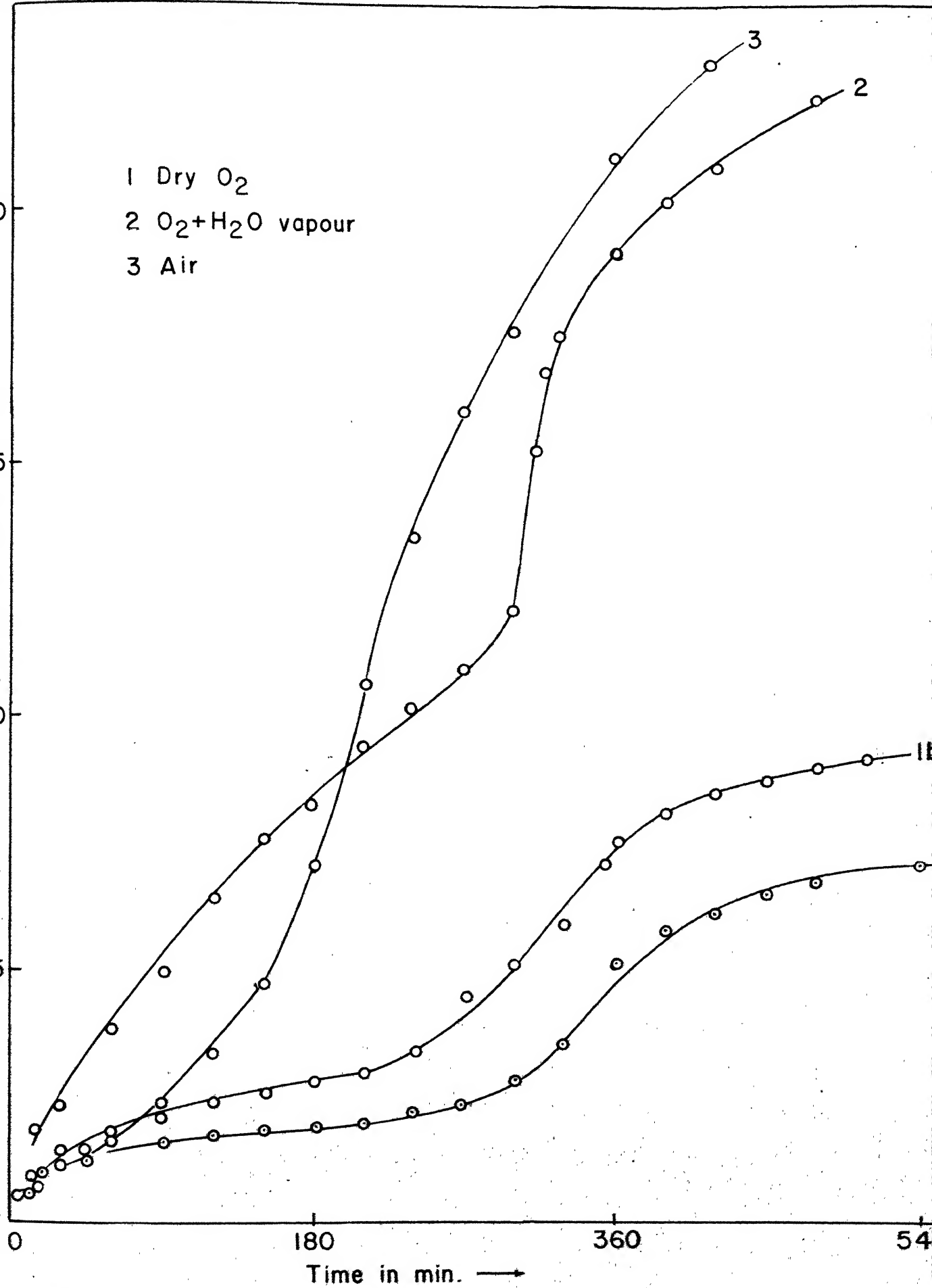


Fig. 3.13 Weight gain vs time plot of 2.5 Cr - 1 Mo steel in different temperatures.



oxygen-water vapour mixture is parabolic initially and changes to some other law later on.

Oxidation in oxygen-water vapour mixture is more at all temperatures than the oxidation in dry oxygen. A comparison in weight gain observed in 10h duration in these environments indicates that this weight gain is about three times higher at 750°C , 1.7 and 1.2 times higher at 850°C and 950°C respectively.

Influence of moisture content on oxidation rate was also carried out. While all the runs in oxygen water vapour mixture were carried out by saturating oxygen gas with 5 pct. water vapours, one run was carried out by saturating it with 10 pct. water vapours. The plot of this run is shown by curve II with dotted marks in Fig. 3.3. One can see the tremendous increase in oxidation rate.

The results at 1000°C are quite interesting. The oxidation rate in air is much more than either in dry oxygen or oxygen-water vapour mixture. From tables 3.1 to 3.3 one can observe that while in both dry oxygen and oxygen-water vapour mixture initially the oxidation occurs parabolically but in air it starts linearly for about hundred minutes or more. After this initial period in all the three cases, a rise in weight gain appears, this region is shown by

a 'n' value of .5 in all the three environments. While this region is quite long in air, smaller in oxygen-water vapour mixture and least in dry oxygen. The oxidation in last two cases i.e. in dry oxygen and oxygen water vapour mixture be termed as breakaway type of oxidation as this sudden increase is observed after an initial protective layer formation, while in air it is termed as catastrophic oxidation. According to Leslie and Fontana⁷ such type of behaviour is expected at high temperatures for most of the alloys which contain Mo, even in very small quantities.

Reported⁸ results for iron-chromium alloys indicate that the oxidation in air is lower than that in pure oxygen. Present work, however shows that the oxidation in air of 2.5 Cr - 1 Mo steel is more in air than in oxygen. This may be due to the fact that the experiment was carried out in laboratory air without removing impurities and moisture.

High oxidation rate in moist oxygen over that in dry oxygen are in agreement with the reported results of some workers⁹⁻¹¹ for iron and iron-chromium alloys while others^{12,13}, indicate either no change or reduction in rate. Rahmel¹⁴ reported that for pure iron at 750°C, the oxidation rate is not influenced by the presence of water vapours, but the scaling rate increases 1-2 times at 850°C

and 1.6 times at 950°C in the presence of moisture.

3.7 Activation Energies:

The Arrhenium plot for both the results in oxygen and oxygen-water vapour mixture is shown in Fig. 3.15. Activation energy for air in parabolic range was calculated using temperature dependence of Arrhenius equation:

$$\Delta E = \frac{R T_1 T_2 \ln K_1 / K_2}{T_1 - T_2}$$

where K_1 and K_2 are the values of parabolic rate constants at temperatures T_1 and T_2 . Values of K_1 and K_2 are given in table 3.1 at 1023°K and 1073°K. The activation energy so calculated was 35.5 Kcal/mole (148.7 KJ/mole). The activation energies for oxidation in oxygen and oxygen-water vapour mixture determined from the plots shown in fig. 3.15 are 24.0 Kcal/mole (100.5 KJ/mole) and 15.4 Kcal/mole (64.5 KJ/mole) respectively. These activation energies can be applied in temperature range 700-900°C in oxygen and 650-850°C in oxygen water vapour mixtures as the points for rate constants above this temperature are highly scattered as shown in the Fig. 3.15. The value of activation energy calculated in the temperature range 900-1000°C comes to be same in both environments i.e. 80.0 Kcal/mole (335 KJ/mole).

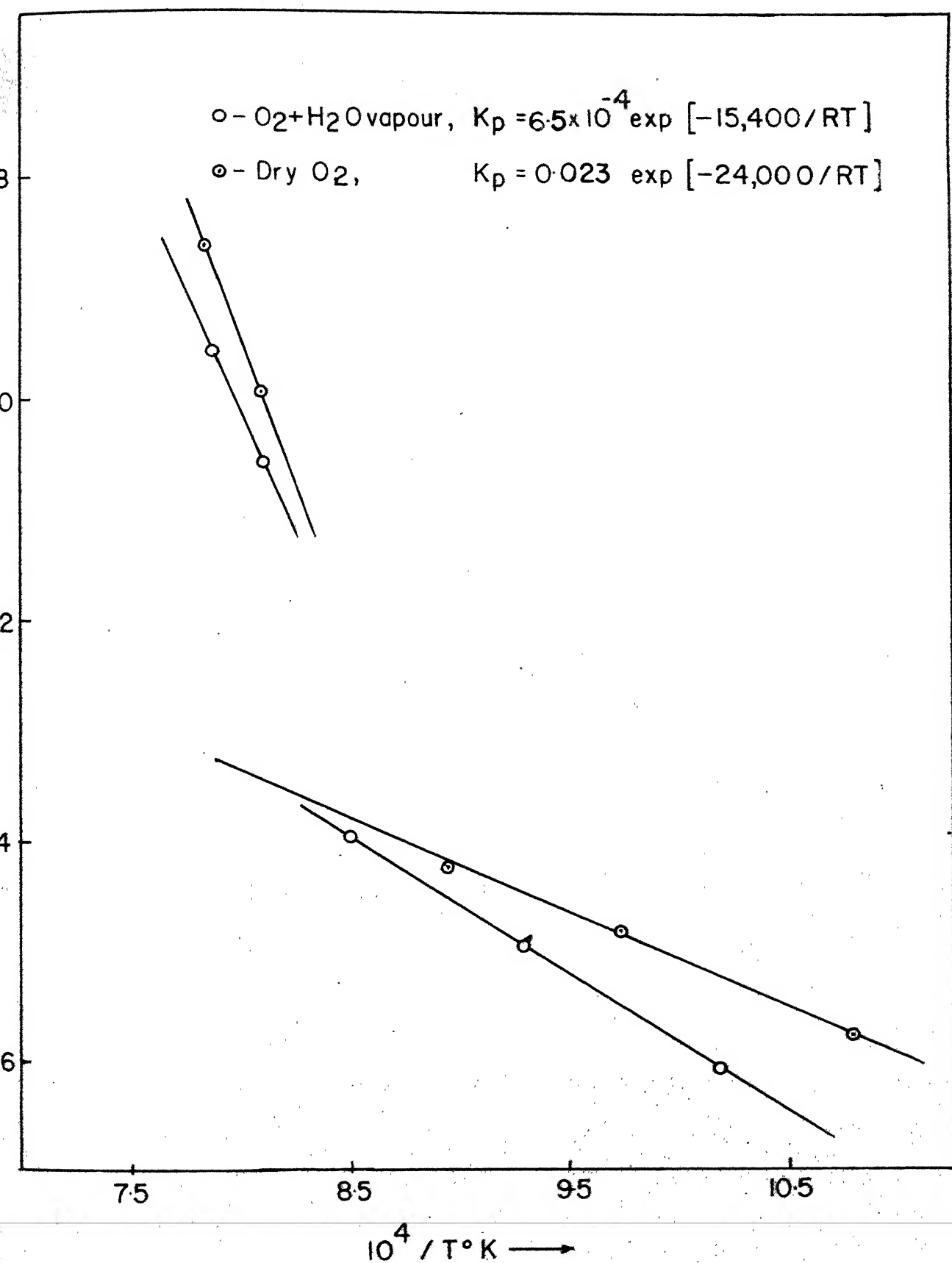


FIG 3.15 Temperature dependence of rate constant

Since the activation energies are different in the three environments, the mechanism of oxidation is expected to be different in these cases. Activation energies above 900°C in both oxygen and oxygen-water vapour mixture is same, thus the mechanism of oxidation at these temperatures may be the same. Further discussion in this respect is restricted in this chapter, as the results of oxidation products are yet to be explained.

The activation energy calculated in the linear range of the oxidation in air is found to be 99 Kcal/mole (414.6 KJ/mole). It is difficult to account for this high value due to the lack of our knowledge about the processes occurring during reaction. However, this high value may be associated with the phase boundary reaction as controlling step after rupture of initial oxide scale. The rupture¹⁵ of scale occurs after certain stress is built.

The activation energies associated with other rate laws in this investigation corresponding to other values of n , given in tables 3.1 to 3.3 cannot be easily related to the processes occurring during the reaction, because mechanisms for such processes are not well understood.

The values of activation energies of oxidation for this particular alloy are not available in literature, hence a comparison could not be made.

References:

1. V.V.Ipatev et al. Uchenye Zapiski Lenigr. Goaundarst Univ., 175, Ser. Khim. Nauk, 14, 88 (1954) Chem. abst. (51) 4240e (1957).
2. D. Caplan and M. Cohen, Corr. 15, 141t (1959).
3. D. Caplan et al., J. electrochemical Soc. 108, 1344 (1961).
4. H.H. Uhlig., Corr. 19 (1963) p. 231-237.
5. Per Kofstad, 'High Temperature Oxidation of Metals' P 16.
6. J. Romanski, Corr. Sc. 8, 67 (1968).
7. W.C. Lesila and M.G. Fontana, Trans. ASM, 41, 1213 (1949).
8. G.C. Wood, Corr. Sc. 2, 173 (1961).
9. D. Caplan and M. Cohen, Corr. 15, 57 (1959).
10. C.T. Fujii and R.A. Meussner, N.R.L. Rept. 5506, 1960.
11. J. Benard et al., Z. Elektrochem., 61, 59 (1957).
12. W.I. Tikhomirov et al., Ber. Akad., Wiss, USSR, 95, 305 (1954).
13. J. Weber, Corr. Sc. 16, 499 (1976).
14. A. Rohmel and J. Toboski, Corr. Sc. 5, 333 (1965).
15. Per Kofstad, 'High Temperature Oxidation of Metals' p. 233-234.

CHAPTER 4

EXAMINATION OF OXIDATION PRODUCTS

4.1 Physical Features:

Last coloumn of the tables 1 to 4 in Appendix 1 lists the physical features of the oxide films observed on the various steel samples.

The oxide film formed in the initial stages was bright violet in colour. A sample which was just dropped in the reaction tube maintained at 800°C , for few seconds and removed appeared bright violet in colour. A comparison of this colour to the colours of the various oxides listed in Appendix 2 suggests the possibility of Cr_2O_3 layer. In air, the oxide film formed at 600°C for 20h duration appeared light grey in colour. Air-oxide oxide film formed in oxygen water vapour mixture at 650°C for 20h duration appears black in colour, suggesting the possibility of FeO or Fe_3O_4 . Air oxide film formed at 1000°C appeared to be bluish-black in colour, while that formed in oxygen and oxygen-water vapour mixture appeared brownsish-black in colour.

The scale appeared to be loose and blistered at low temperatures. Adherence was very poor at these temperatures. It used to fall off during the unloading of specimen.

On the other hand scale formed at high temperature was quite thick and had better adherence to the alloy. Oxide films formed for short durations at low temperature appeared quite uniform, smooth and highly adhering to the surface. Oxide films from such samples were removed by the dissolution technique. A 5 pct. Br_2 solution in methanol was used for this purpose. It does not affect the oxide scale, but can dissolve the matrix. Fig. 4.1 shows three samples, finally polished specimen ready for oxidation studies is shown on extreme left, oxidised specimen with oxide layer intact on its surface, in the middle, and on extreme right is shown a sample whose oxide layer had been stripped off using dissolution technique.

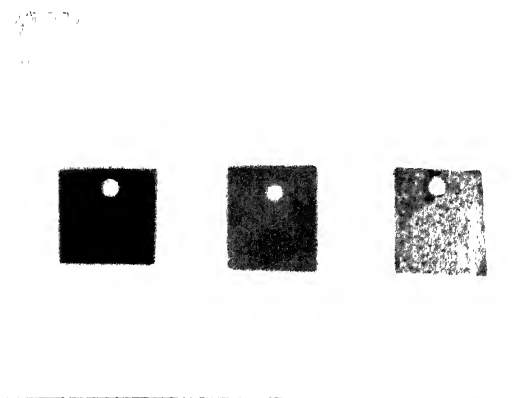


Fig. 4.1

4.2 Optical Microscopy

Figs. 4.2 to 4.20 show the micrographs for the cross-section of various samples taken on an optical microscope. Magnification for each micrograph is given on the right corner of the fig.

Fig. 4.2 to 4.4 compares the scale thickness formed in air at temperatures 750°C , 850°C and 950°C for 18h exposure. Thus the results are in agreement with the thermogravimetric results, that the oxidation increases with increase in the temperature of oxidation. Fig. 4.8 to 4.10 and 4.13 to 4.16 in a similar fashion compare the oxide scale in oxygen and oxygen water vapours respectively. Oxide scale at 850°C shown in fig. 4.13 is thicker than the oxide scale at 950°C shown in fig. 4.14. This is because former was oxidised in oxygen 10 pct. water vapours and latter in 5 pct. water vapours. The results are in agreement with those obtained during thermogravimetric investigations.

Fig. 4.5, 4.6, 4.11, 4.12, 4.16 and 4.17 show the edge effect. Micrograph shown in fig. 4.7 depicts the catastrophic oxidation at 950°C . This again confirms the results by thermogravimetric investigations that rate of oxidation is very fast at this temperature and occurs linearly.

Micrographs shown in figs. 4.12A, 4.18 to 4.19 show the oxide scale at higher magnification. Although much information cannot be gathered from these micrographs except the oxide layer thickness and number of oxide layers formed. Fig. 4.4 indicates that oxide scale formed in air at 950°C consists of three layers and that 850°C consists of two layers. In oxygen environment as shown by fig. 4.8 to 4.10 the scale appears to be single layered only while in oxygen-water vapour mixture it appears to be of two layers.



X 66

Fig. 4.2 Cross-section at 750°C



X 66

Fig. 4.3 Cross-section at 850°C



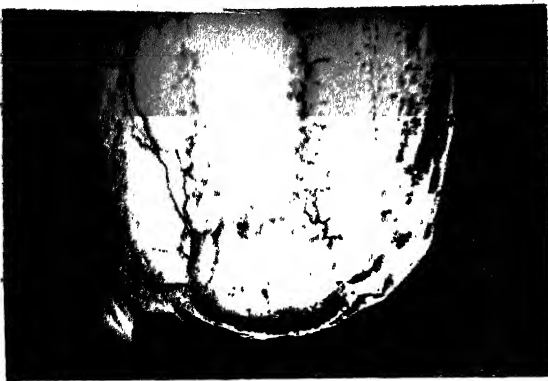
X66

Fig. 4.4 Cross-section at 950°C



X66

Fig. 4.5 Edge effect at 850°C



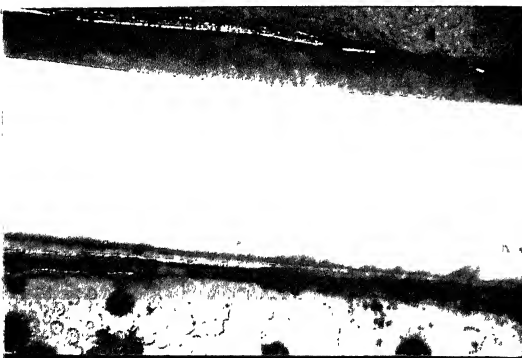
X66

Fig. 4.6 Edge effect at 950°C



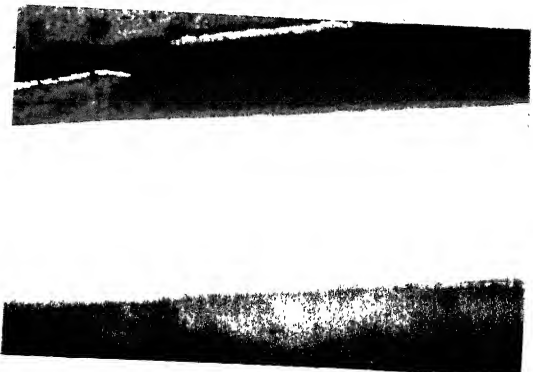
X66

Fig. 4.7 Necking portion at 950°C



X66

Fig. 4.8 Cross-section at



X66

Fig. 4.9 Cross-section at



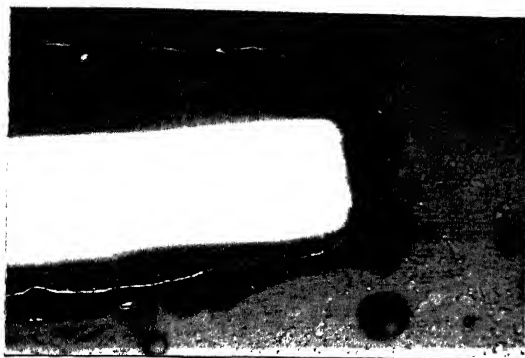
X66

Fig. 4.10 Cross-section at 950°C



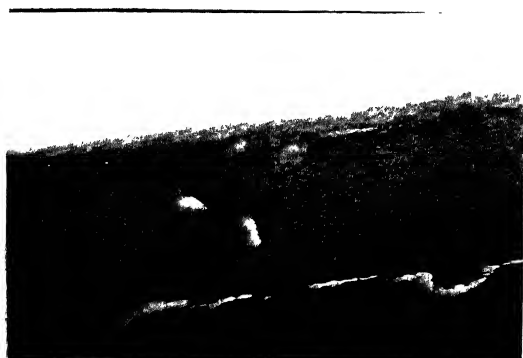
X66

Fig. 4.11 Edge effect at 850°C



X66

Fig. 4.12 Edge effect at 950°C



X66

Fig. 4.12A Oxide layer at 950°C



X66

Fig. 4.13 Cross-section at



X66

Fig. 4.14 Cross-section at



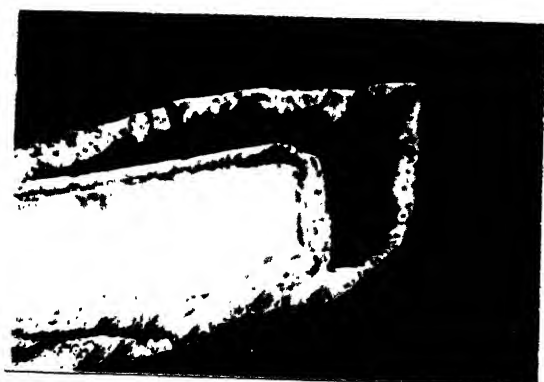
X66

Fig. 4.15 Cross-section at 1000°C



X132

Fig. 4.16 Edge effect at 850°C



X66

Fig. 4.17 Edge effect at 1000°C



X266

Fig. 4.18 Oxide layer at 850°C



X266



X132

4.3 Scanning Electron Microscopy:

Air oxidised scales were studied using SEM.

Fig. 4.21 shows a micrograph for the cross section of a sample at 950°C . Corresponding optical micrograph was shown in fig. 4.4, which revealed that oxide scale consists of three layers. But the SEM micrograph clearly indicates that the scale consists of a single layer and the black lines seen in the scale are cracks. These cracks are further shown more clearly at a higher magnification in fig. 4.22.

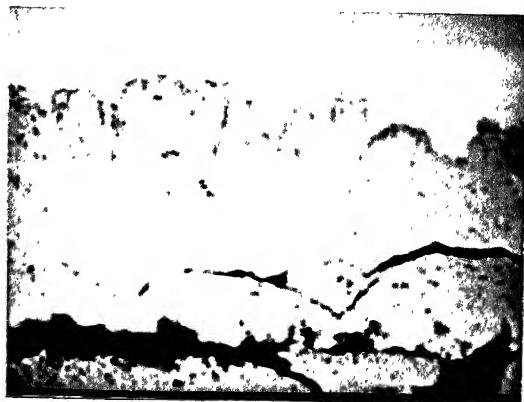
Catastrophic oxidation at 950°C is very clearly shown in fig. 4.23. In this figure the necking portion is focussed. Fig. 4.24 shows this necking portion at much higher magnification. This photomicrograph reveals how porous the oxide layer^{is} and how loosely it is attached to the matrix.

Fig. 4.25 reveals the SEM photograph of the oxide scale at 850°C . It confirms the information revealed by optical micrograph that the scale at this temperature consists of two layers.



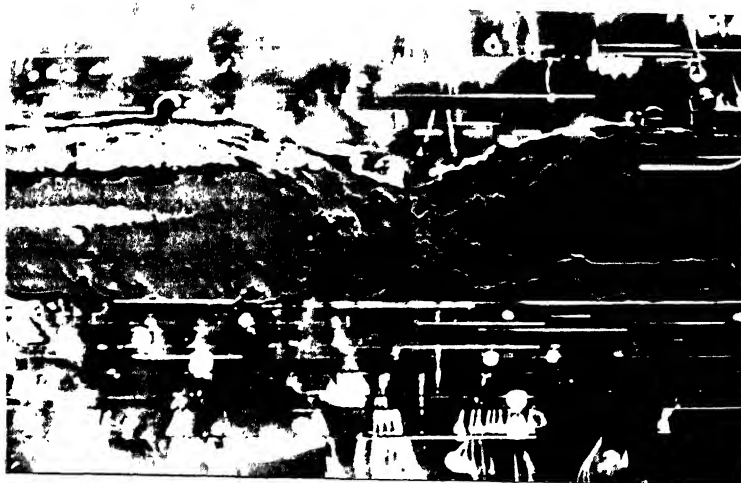
X160

Fig. 4.21 Oxide layer at 950°C



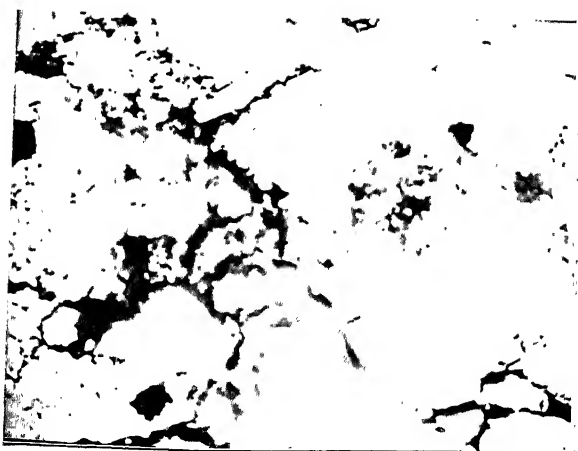
X640

Fig. 4.22 Oxide layer at 950°C

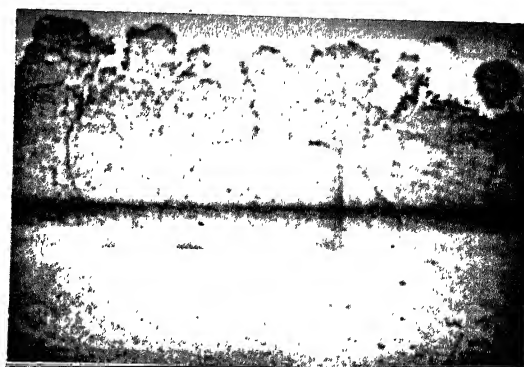


X52

Fig. 4.23 Necking portion



X320



X640

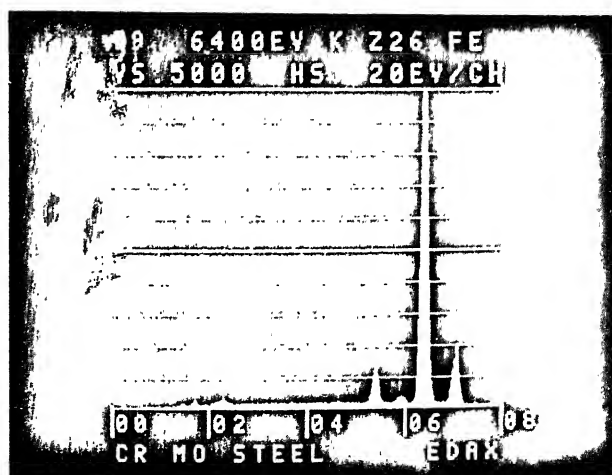
4.4 EDAX (Energy Dispersive X-ray Analysis):

Concentration profiles for the constituents of the alloy were taken throughout the scale thickness on air oxidised samples. These are shown in fig. 4.26-4.28 for the oxide scale at 950°C, 850°C and 750°C. Intensity vs energy plots have been shown at various spots throughout the scale thickness. The E values where the peaks for Fe(K α), Mo(L α) and Cr(K α) appears are 6.40, 2.29 and 5.41 KeV respectively. In fig. 4.26, plot a reveals the concentrations of Cr, Mo and Fe on the unattacked matrix. Plot b was taken very near to the matrix and plots c and d were taken 160 μ and 300 μ away from the matrix. Thus it appears that the concentration of the various constituents are not same throughout the scale, though a single uniform scale is shown by SEM micrograph. This result reveals that chromium is concentrated near to matrix. As oxide thickness increases it is mainly the iron in the scale. In other words we can say that chromium diffuses to the matrix and Fe towards the oxide scale. Thus more and more iron is available for oxidation.

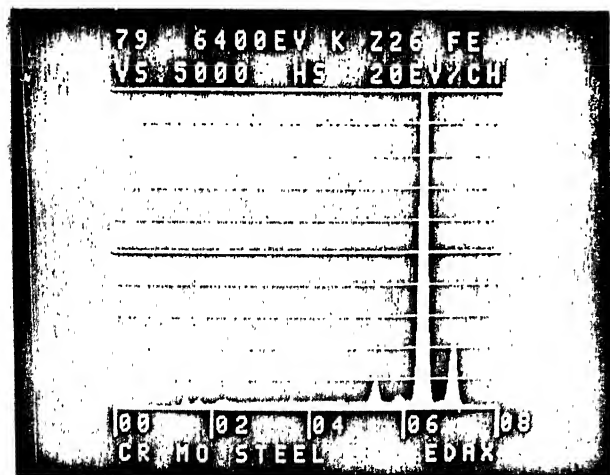
At 850°C, SEM micrograph shows two distinct layers. EDAX analysis shows that the inner layer (fig. 4.27b) is rich in both chromium and iron and hence this layer may be due to some mixed oxide of iron and chromium. In outer



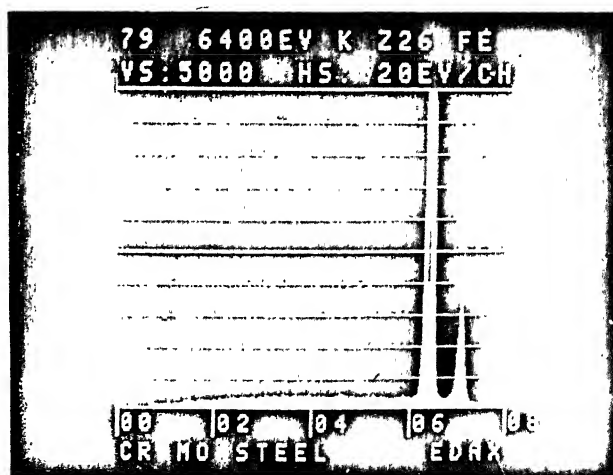
a



b

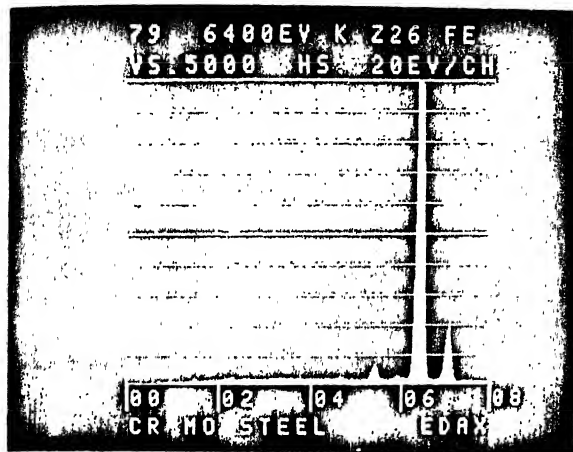


c

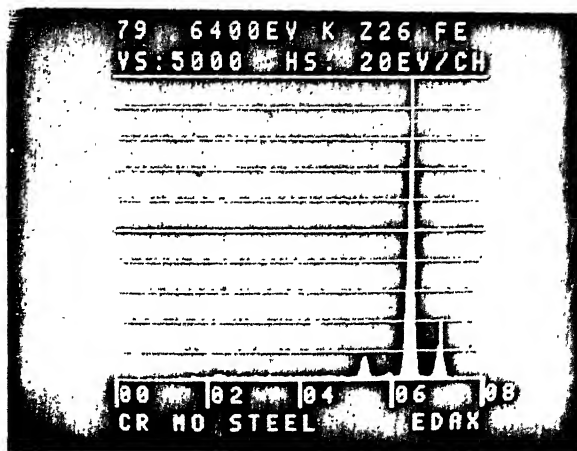


d

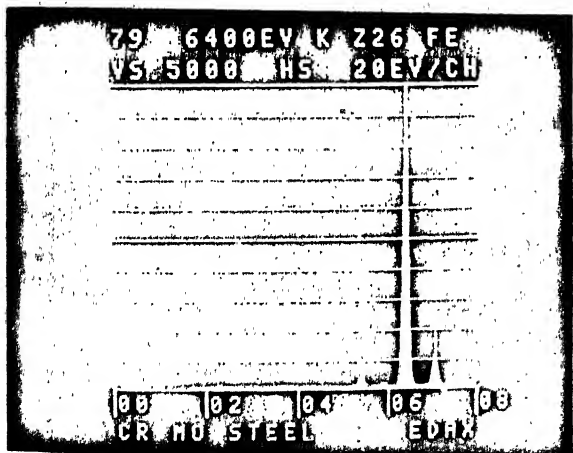
FIG.4.16 EDAX analysis of oxide layer at 950°C



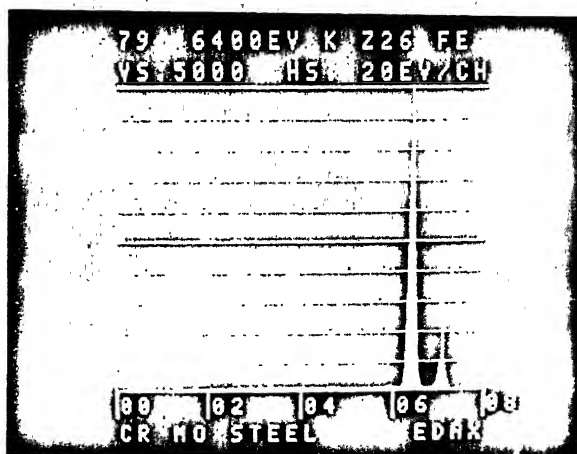
a



b

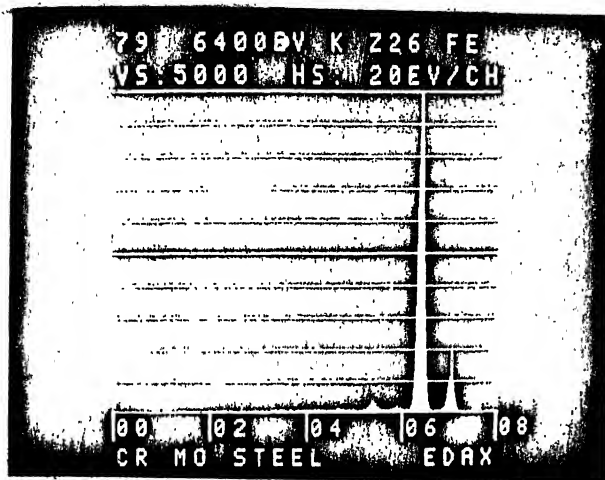


c

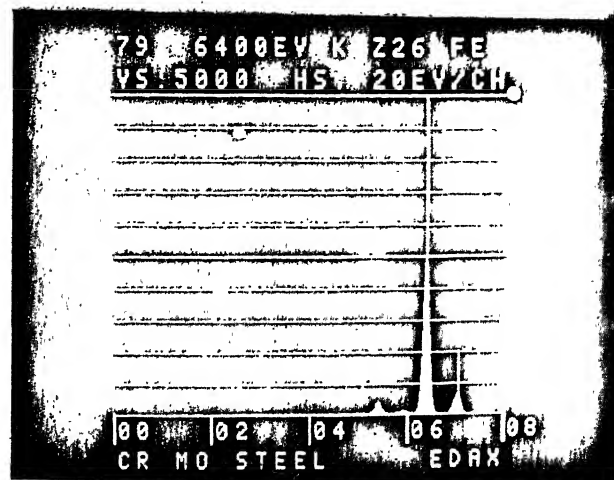


d

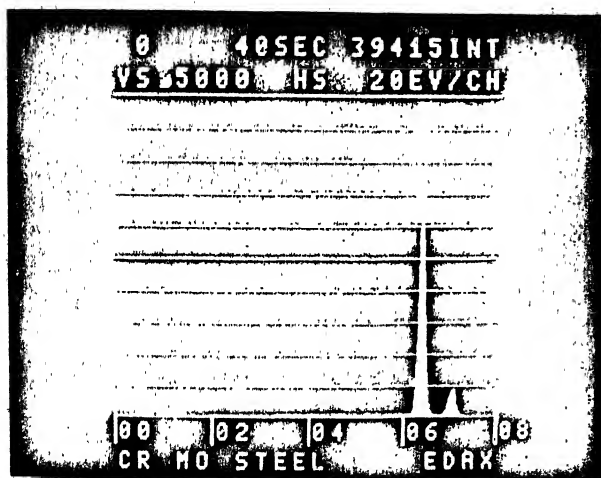
FIG.4.27 EDAX analysis of oxide layer at 850°C



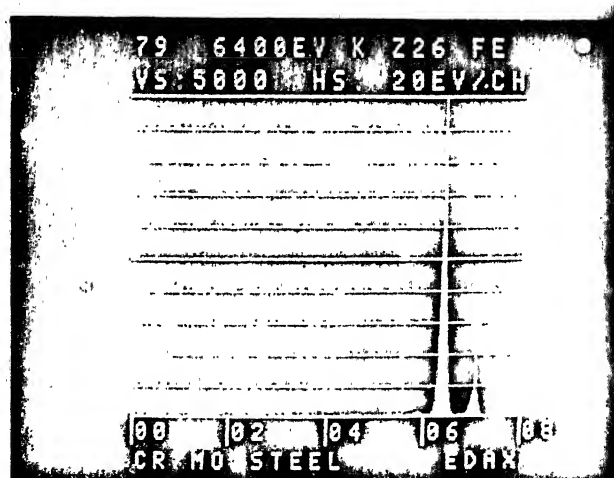
a



b



c



d

FIG.4.4 EDAX analysis of oxide layer of 750°C

layer Cr is present just on the boundary of two layers. While it is mostly iron afterwards. Thus the second layer must be an oxide of iron only.

At 750°C, oxide scale was found to be only 25μ thick as compared to 300μ thick at 850°C. Oxide scale at 950°C was thicker than at 850°C but could not be measured accurately, as it spalled off during mounting and polishing. EDAX results are shown for oxide scale at 750°C in fig. 4.28. This indicates that the scale is rich in iron mainly, but small concentration of chromium are present near to the matrix.

4.5 X-ray Diffraction Analysis:

X-ray diffraction runs were taken for number of samples. Table 4.1 gives the detail for various samples analysed. Coloumn one gives the sample details, coloumn two gives the 2θ values for various peaks observed during the diffraction run. Corresponding 'd' values have been listed in third coloumn and the pct. intensity ratio in 4th coloumn. These 'd' values have been compared with those listed in the X-ray diffraction data files and hence the corresponding compound was identified. Appendix 2 lists the 'd' values for some of the important compounds useful for this analysis. Coloumn five in this table names the most appropriate compound

identified. It is necessary to add here, that the oxide layers formed are not the compound of a single constituent. It can be either a mechanical mixture of two or more compound, a mixed oxide, a solid solution, or an impure oxide i.e. an oxide whose lattice positions have been occupied by other elements. Since the X-ray Diffraction data file lists the 'd' values for only pure compounds, hence an exact peak to peak match was not possible. The results that have been suggested in the fifth column of the table have been obtained by matching the important peaks of the compound identified. Further on arriving at these results, the information obtained already from optical and SEM was utilised.

At 750°C air oxide film is made of $\alpha\text{-Fe}_2\text{O}_3$ only. This are in agreement with EDAX results where it was shown that scale mainly consists of iron only. Since small concentration of chromium were detected in the scale hence the oxide Fe_2O_3 is not pure one, but an impure one i.e. some Cr may have replaced Fe in the Fe_2O_3 lattice. That is the reason why there is slight shift in the main peaks for $\alpha\text{-Fe}_2\text{O}_3$.

At 850°C, x-ray result indicate the presence of $(\text{Fe,Cr})_2\text{O}_3$ and $\text{-Fe}_2\text{O}_3$ in the scale. This is again in agreement with EDAX and SEM results. Thus the inner layer may be of $(\text{Fe,Cr})_2\text{O}_3$ and outer layer of $\text{-Fe}_2\text{O}_3$.

Table 4.1

Sample Detail	2 θ	Corres- ponding 'd' value	Intensity	Compound(s) Identified
No. 69	28.4	3.1399		α -Fe ₂ O ₃
	29.2	3.0557	40	
Temp. 750°C	30.5	2.9283		
	32.8	2.7281	100	
	35.2	2.5474	60	
	44.4	2.0385	20	
	53.8	1.7025	70	
	62.2	1.4912	30	
	63.4	1.4659	30	
No. 12	22.8	3.8969		
Temp. 800°C	24.0	3.7047	30	(Fe,Cr) ₂ O ₃ and
	30.2	2.9568	30	-Fe ₂ O ₃
	32.2	2.7775	20	
	33.2	2.6961	50	
	35.6	2.5196	100	
	43.0	2.1016	30	
	49.5	1.8398	40	
	54.2	1.6909	55	
	62.3	1.4890	60	
	64.0	1.4535		
	73.0	1.2949		

Sample Detail	2 θ	Corres- ponding 'd' value	Intensity	Compound(s) identified
No. 26	24.5	3.6302		(Fe,Cr) ₂ O ₃ and -Fe ₂ O ₃
Temp.	30.2	2.9568		
850°C	32.4	2.7608	30	
	33.6	2.6649	80	
	36.1	2.4859	100	
	49.0	1.8574		
	50.0	1.8226		
	54.5	1.6822	50	
	56.4	1.6300		
	62.9	1.4763	55	
	64.5	1.4434	80	
	66.0	1.4143		
	70.2	1.3395		
	72.4	1.3042		
No. 58	27.9	3.2018		α -Fe ₂ O ₃
Temp.	33.2	2.7120	80	
950°C	35.6	2.5190	95	
	40.8	2.2077	30	
	54.0	1.6966	50	
	62.4	1.4869	65	
	63.8	1.4568	100	

Sample Detail	2 θ	Corres- ponding 'd' value	Intensity	Correspond(s) Identified
No. XXVI	30.1	2.9664		
Temp.	33.4	2.6804	40	
600°C	36.0	2.4926		
	40.3	2.2360	80	
	45.0	2.0127	100	
	54.0	1.6966	30	
	65.2	1.4912	35	
No. 88	24.8	3.5870		Cr ₂ O ₃
Temp.	30.4	2.9377		
800°C	32.8	2.7281		
	33.8	2.6496	100	
	36.2	2.4793	95	
	41.4	2.1791	40	
	50.0	1.8226	50	
	54.6	1.6794	60	
	62.0	1.4955	40	
	63.5	1.4638	30	
	71.7	1.3152		

Sample Detail	2 θ	Corres- ponding 'd' value	Intensity	Compound (s) Identified
<hr/>				
No. IV	25.5	3.4901		Fe ₂ O ₃ , Cr ₂ O ₃
Temp.	26.5	3.3606		
900°C	29.0	3.0763		
	31.0	2.8823		
	32.4	2.7608	30	
	33.4	2.6804	100	
	35.9	2.4993	85	
	41.2	2.1892		
	49.9	1.8260	70	
	54.4	1.6851	70	
	62.8	1.4784	40	
	64.4	1.4455	60	
<hr/>				
No. XXII	30.4	2.9377		
Temp.	32.2	2.7775		
1000°C	35.7	2.5129	80	
	56.2	1.6353		
	57.4	1.6040	40	
	62.8	1.4784	100	

Sample detail	2 θ	Corresponding 'd' value	Intensity	Compound(s) Identified
No. W5	24.0	3.7047		
Temp.	30.0	2.9760	30	Fe_3O_4
650°C	31.9	2.8029		
	33.1	2.7040	70	
	35.4	2.5334	100	
	49.4	1.8433		
	54.0	1.6966		
	57.0	1.6142	40	
	62.4	1.4869	65	
	64.0	1.4535	30	
No. W1	24.6	3.6157		
Temp.	33.4	2.6804	70	FeCr_2O_4
750°C	35.8	2.5060	80	
	50.0	1.8226		
	54.6	1.6794	50	
	58.4	1.5789		
	58.8	1.5691		
	59.8	1.5452		
	63.0	1.4742	100	

Sample Detail	2 θ	Corres- ponding 'd' value	Intensity	Compound (s) Identified
No. W8	25.0	3.5587		FeCr_2O_4
Temp.	26.2	3.3784		
850°C	30.4	2.9377		
	33.4	2.6804	95	
	35.8	2.5060	100	
	46.2	1.9632		
	48.8	1.8645		
	49.8	1.8294		
	54.5	1.6822	50	
	57.7	1.5963		
	62.7	1.4805	80	
	64.4	1.4455	60	
No. W7	24.6	3.6157		Fe_2O_3
Temp.	30.4	2.9377		
900°C	32.4	2.7608	30	
	33.5	2.6727	100	
	35.9	2.4993	80	
	50.0	1.6794		
	54.6	1.8226	70	
	63.0	1.4742	60	
	64.6	1.4414	50	
	72.5	1.3026		

At 950°C again the results are in agreement with that predicted by SEM and EDAX results. Shifting in the peaks and missing of some peaks of Fe_2O_3 may be due to the presence of Cr in the lattice of Fe_2O_3 .

Oxide layer formed at 600°C in dry oxygen did not match with any oxide or mixed oxide of Fe, Cr or Mo. But it slightly matched with an intermetallic compounds of three element the sigma CrFeMo, whose 'd' values are given in appendix 2. Possibility of no oxide formation confirms the thermogravimetric investigations that oxygen uptake was very small at this temperature.

Formation of Cr_2O_3 at 800°C confirms the thermogravimetric results carried out in various oxygen pressures. A $P_{\text{O}_2}^{1/2}$ dependence on oxygen pressure indicated the possibility of a p-conducting scale. Since Cr_2O_3 is p-conducting, thus results are in agreement. A slight shift in the values of some peaks may be due to the presence of impurities or other oxides.

Oxide layer at 1000°C in oxygen could not be identified clearly, but it appears to be Fe_2O_3 .

Formation of Fe_3O_4 at 650°C in oxygen water-vapour mixture confirms the results obtained while colour examination. A black layer formed could be of Fe_3O_4 .

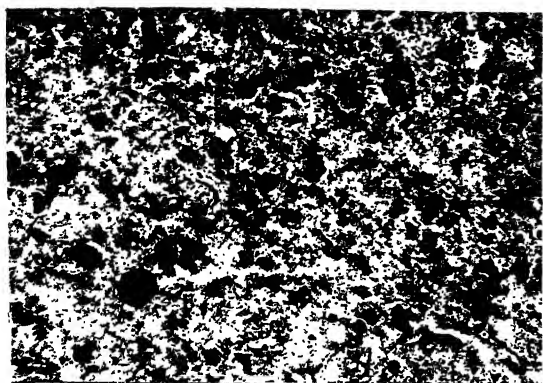
Formation of FeCr_2O_4 at intermediate temperatures seems to be in agreement with the results reported by many workers. FeCr_2O_4 is nothing but $[\text{FeO}.\text{Cr}_2\text{O}_3]$, formation of FeO in oxide scales in presence of moisture is reported by above workers.

At high temperatures formation of Fe_2O_3 as indicated by x-ray results seems to be justified as at high temperatures, since the activation energies are same for both oxygen and oxygen-water vapour mixture, thus mechanism of oxidation should be same.

However much more rigorous analysis is needed to confirm the above mentioned results.

4.6 Electron Microscopy:

Very few samples which were oxidised for very short duration were observed in electromicroscope. Fig. 4.29 shows the surface topography of an air oxidised sample at 500°C for 10h duration. Corresponding electron diffraction pattern is shown in fig. 4.30. Fig. 4.31 shows the topography of an oxide formed in air at 800°C for 15 minute duration. It appeared to be needle like shapes as shown in fig. 4.32. Corresponding electron diffraction pattern is shown in the fig. 4.33.



X13000

Fig. 4.29 TEM PICTURE at 500°C

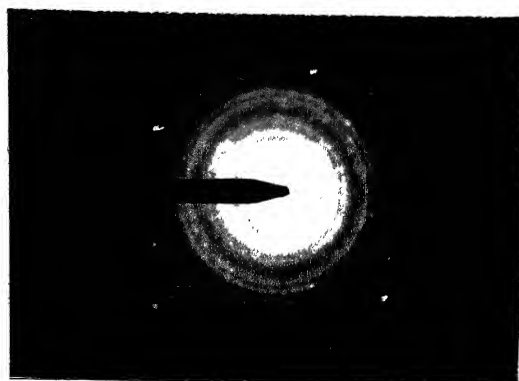
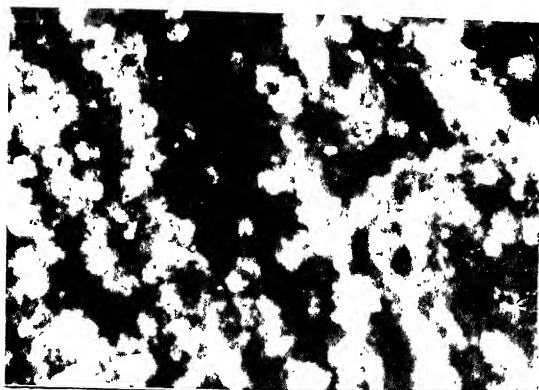


Fig. 4.30 Electron diffraction pattern of oxide layer at 500°C.



X13,000

Fig. 4.31 TEM PICTURE at 800°C



Fig. 4.32 Electron diffraction pattern at 800°C.



x22,000

Fig. 4.33 Oxide structure at 800°C revealing needle type shape of oxide growth in initial stage.

CHAPTER 5

GENERAL DISCUSSION AND CONCLUSION

So far the results of thermogravimetric experiments and the examination of the oxidation products have been presented. In this chapter an attempt is made to relate these observations to some suitable mechanism.

It is discussed earlier that the low temperature oxidation follows logarithmic kinetics. There are several mechanisms proposed to explain such behaviour. The best suited to our results is that proposed by Uhlig¹ which is applicable to thin films of thickness less than $10,000 \text{ \AA}$. Mott-Hauffe and Ilschner² proposed a theory which could be applicable to thin films less than 50 \AA . Since the film thickness on the samples in logarithmic range was in the range of 2500 \AA to 7000 \AA , thus Uhlig's theory is most suitable to explain the mechanism. According to this theory electron transfer at the metal oxide interface determines the oxide growth.

The parabolic oxidation is observed in intermediate temperature range in air, and in initial stages at all temperatures in oxygen and oxygen water vapour mixture. Since the activation energies for parabolic oxidation are different in all three environments, thus the mechanism of the oxidation is

expected to be different in all the three cases. This has been confirmed by x-ray results which indicate different compositions of oxide scales in three environments. In air oxidation, Fe_2O_3 is formed which is an n-type semiconductor hence the mechanism of oxidation is due to the oxygen diffusion to the metal scale interface via vacant anion sites. In case of oxygen oxidation, the scale consists of Cr_2O_3 which ^{is} a p-type semiconductor hence the mechanism of oxidation is due to the diffusion of either cation vacancies or of interstitial oxygen ions from the surface to the interface. If the vacancies migrate towards the interior they must accumulate near the metal-oxide interface and eventually precipitate in the form of blisters or holes. Such blisters were observed on the scales formed on samples oxidised in oxygen.

High oxidation rate of the alloy in air can be explained as follows. According to Lubaschewski³ when an n-type oxide is formed, presence of nitrogen would increase the number of vacant oxygen sites and increase the oxidation rate. Since in air oxidation Fe_2O_3 is formed which is n-type, thus increase in oxidation rate in air is justified. Arkharov and Luchkin⁴ interpreted high oxidation rate of Ti in air (at 1100°C) as compared with that in pure oxygen, due to the formation of TiO_2 which is n-type. both at 1 atm. pressure/ Chromium oxide on the other hand

is a p-type semiconductor, and in air therefore the rate of scale formation is reduced as compared with oxygen⁵.

Linear oxidation rate at high temperature as observed in air, can be explained by Cabrera-Mott⁶ theory, according to which if an n-type oxide is formed, then this linear rate may be due to the ion transfer in the electric field. Catastrophic oxidation observed at this temperature in air may be explained by the increasing rate of oxidation as time elapses. This increasing rate of oxidation is due to some phase-boundary reaction as explained by Kofstad⁷, after the rupture of the scale. Such rupture of the scale was shown by some of the SEM micrograph.

Break away oxidation observed in the case of oxygen and oxygen water vapour mixture can be explained by the theory of non-uniform scale. Formation of non-uniform scale, that is porous or cracked scale, is to some extent connected with Pilling-Bedworth rule⁸. This rule is very important for scales in which diffusion of matter is from the surface towards the metal scale interface, for instance for oxides, /_of the n-type in which oxygen diffuses via cation anion sites. Here since Fe_2O_3 is formed at these temperatures, thus the following oxidation mechanism seems to be the most suitable. Oxygen ions diffuse from the surface to the metal oxide interface, where they form new oxide which owing to

its high volume ratio : expands against the resistance the existing oxide layer, and severe biaxial stresses develop which eventually lead to rupturing of film. Simultaneously oxygen dissolves in the metal. Thus an initial parabolic growth turns into a linear one. Such type of observations have already been confirmed by many workers^{9,10} on niobium tantalum alloys.

High oxidation rate in oxygen water vapour mixture is not well understood. Only theory presently available is from Rahmel¹¹ on oxidation on pure iron. According to this theory, in presence of water vapours a H_2/H_2O mixture is formed in the pores which transports by an oxidation reduction mechanism, oxygen to iron surface. Therefore oxide bridges are built up from the metal to scale which enables the further oxidation of metal without substantial inhibition.

Conclusion

1. Oxidation in air was found to be logarithmic at low temperatures, parabolic and cubic in intermediate temperatures and linear at high temperatures. The oxidation at high temperature was described as the catastrophic oxidation. The activation energy for the parabolic oxidation in air was determined to be 35.5 Kcal/mole.

2. Oxidation in dry oxygen was found to be logarithmic at 600°C for a very short time, after which the rate fell to almost zero. Oxidation above this temperature was parabolic in beginning and switched over to some other law after some time. This initial parabolic range was longer at low temperatures and decreased as the temperature of oxidation increased. Breakaway oxidation was observed at 1000°C. Parabolic oxidation in oxygen could be described by following equation

$$K_p = 0.023 \exp (-24,000/RT)$$

in temperature range 700°C-900°C.

3. Oxidation kinetics in oxygen water vapour mixture were observed to be similar to that in dry oxygen. The oxidation in parabolic range could be described by equation

$$K_p = 6.5 \times 10^{-4} \exp (-15,400/RT)$$

in temperature range 650°C-850°C.

4. Oxidation in air was found to be more than ⁱⁿdry oxygen at all the temperatures, but lower than that in oxygen water vapour mixture below 850°C.
5. Oxidation in oxygen-water vapour mixture was found to be more than that in dry oxygen at all the temperatures.

References

1. H.H. Uhlig, Acta metallurgy, 4 (1956) 51.
2. K. Haufee and B. Ilschner, Z. Elektrochem. 58 (1954) 382.
3. O. Kubaschewski and B.E. Hopkins, 'Oxidation of Metals and alloys' p. 92.
4. V.I. Arkharov and G.P. Luchkin, C.R. Acad. Sci., USSR, 83 (1952) (83).
5. V.I. Arkharov et al., Fiz. Metal. i. Metalloved, Akad. Nauk. SSSR 5 (1957) 190.
6. C. Wagner and K. Grunewald, Z. Phys. Chem. 40 (1938) 455.
7. P. Kofstad 'Oxidation of Metals at High Temperatures' p. 233.
8. O. Kubaschewski and B.E. Hopkins 'Oxidation of Metals and alloys' p. 40.
9. J.V. Cathcart, J.J. Campbell and G.P. Smith, J. Electrochem. Soc. 105 (1958) 442.
10. J.V. Cathcart, R. Bakish and D.R. Norton, ibid 107 (1960) 668.
11. A. Rahmel and J. Tobolski, Corr. Sc., 5, 333 (1965).

CHAPTER 6

NEED OF FUTURE WORK

Present work is a preliminary attempt towards the understanding of oxidation kinetics of 2.5 Cr - 1 Mo steel in air, oxygen and oxygen-water vapour mixture. However a large number of queries are still unsolved. Hence a good amount of work is needed to understand various concepts more clearly. Some of these are worth mentioning.

1. Mechanism of oxidation in logarithmic range is proposed to be due to ion-transfer in electric field. A systematic study in thin film range is needed, in order to understand these processes more clearly.
2. Oxidation in parabolic range has been attributed to the diffusion of vacancies, or interstitials through the oxide scale. In the case of complex scales, formed on the surface, such mechanism is unable explain^{to} the behaviour clearly. Thus an attempt is necessary to develop mechanism where the process of diffusion through complex scales can be explained more clearly.
3. Break-away oxidation occurs when a critical thickness reaches, beyond which the cracking or rupture of protective scale appears and this leads to linear oxidation rate. In present work such breakaway point has been found at 1000°C

after an oxidation time of 352 sec. This corresponds to an oxide thickness of 10μ and 25μ in oxygen and oxygen water vapour mixture respectively. Thus experiments should be performed at temperature lower and higher than 1000°C to find out whether breakaway appears when this critical oxide thickness reaches at these temperatures.

5. The mechanism of the oxide growth needs to be studied in great detail. For this one has to work in thin film region, where the use of electron microscope, LEED or latest instruments for surface analysis like ESCA, Auger Electron spectroscopy can be of great help.

6. The identification of oxide layers using x-ray diffraction method needs further work. A simplified technique is needed to identify often complex scales formed on alloys. Electron probe microanalysis would be of great help.

7. Since linear oxidation is pressure dependent, ~~thus~~ experiments are needed to be carried out in this range at various air pressures to find out pressure dependence on linear oxidation rate.

APPENDIX 1

TABLE - I

Sample No.	Temperature	Surface finish	Duration (min.)	Surface Area/Thickness mm^2/mm	Weight gain (mg/mm^2)	Physical appearance
35	500°C	4/0	540	210 .35	.00190	Very thin violet colour oxide layer, highly uniform and adherent.
47	600°C	4/0	600	120 .52	.00458	Dark Grey coloured, thin and very loose, layer and Brittle oxide layer.
31	650°C	4/0	650	143 .40	.00489	Dark Grey coloured, thin, very loose but non-brittle oxide layer.
42	700°C	4/0	360	160 .35	.00406	-do-
43	750°C	4/0	450	161 .35	.00590	Light Grey, uniform, adherent oxide layer.
33	850°C	4/0	600	189 .35	.0124	-do-
34	900°C	4/0	480	195 .35	.0164	-do-
38	950°C	4/0	360	196 .35	.126	Very light grey, uniform thick, oxide layer.
40	1000°C	4/0	480	184 .35	.248	Dark blue-black thick oxide layer with grey spots on surface.

TABLE - II

No.	Temperature	Surface finish	Duration (min)	Surface Area/	Weight Gain	Physical appearance
				thickness mm ² /mm	Δm mg/mm ²	
	800°C	Rough Polished (on belt)	510	169 .27	.0183	Light Grey, uniform oxide layer.
	800°C	1/0	600	120 .50	.00864	Light Grey, uniform adherent oxide layer.
	800°C	1/0	390	168 .52	.00922	-do-
	800°C	Aluming Polished	600	180 .52	.012	Very thin, Grey Coloured, non-adher- ed oxide layer.
	800°C	-do-	540	154 .52	.00922	-do-
	800°C	4/0	600	160 .35	.0103	Grey coloured, uniform, adherent oxide layer.
	800°C	Electro- Polished	540	120 .52	.0079	Grey coloured, non-uniformly adherent oxide.

Table No. 3

Sample No.	Temperature °C	Duration min.	Surface Area/Thickness mm ² /mm	Weight gain (Δm) mg/mm ²	Physical appearance
XXVI	600	360	170/0.37	2.35×10^{-3}	Surface got tarnished by a very thin, uniform layer, giving violet brownish colour.
XXV	700	720	170/0.37	8.53×10^{-3}	Very thin, highly brittle, light grey coloured oxide layer
XVI	800	990	180/0.35	0.0172	Dark grey, uniform brittle oxide layer.
XXIII	900	720	170/0.32	0.0194	Light grey thin brittle oxide layer
XX	950	600	234/0.32	0.0257	Light grey coloured uniform but brittle oxide layer.
XXII	1000	600	212.5/0.375	0.099	Dark black oxide layer, separating from metal surface as an independent layer.

Table No. 3A

Sample No.	Oxygen pressure mm Hg	Dura- tion	Dimensions/ Thickness mm ² /mm	Weigh gain (Δm) mg/mm ²	Physical Appearance
P6	240	560	160/0.35	0.0118	Slight tarnishing on the metal surface giving violet lynch.
P9	360	600	178/0.31	0.0182	Light grey colour oxide layer uniformly distributed over the surface.
P10	460	600	170/0.35	0.0173	A very light grey thin oxide layer, uniformly distributed over the surface.
P4	530	560	161.5/0.375	0.0198	Dark grey coloured, oxide layer, looking quite rough.
P7	650	600	180/0.35	0.0205	Dark grey coloured, oxide layer, non-uniformly distributed over surface.
P8	760	600	180/0.35	0.0233	Dark grey coloured oxide layer highly adherent to the surface.

Table No. 4

Sample No.	Temperature °C	Duration min.	Dimensions/ Thickness mm ² /mm	Weight gain (Δm) mg/mm ²	Physical Appearance
W5	650	1060	180/0.35	9.99×10^{-3}	Dark grey colour tarnishing on the surface having violet tinch
W1	750	1080	180/0.35	0.0188	Dark grey colour oxide layer, highly brittle and non-sticking to metal surface.
W2	850	1020	176/0.31	0.160	Dark grey colour uniform, thick oxide layer
W8	850	1080	180/0.375	0.0366	Light grey colour, blistered oxide layer
W3	950	1080	187/0.35	0.0422	Dark grey colour adherent oxide layer
W4	1000	480	180/0.37	0.212	Dark bluish, black, rough, very thick oxide layer, adherent to metal surface.

TABLE NO.5.

VI

Thermogravimetric Data.

Table 5.1		Sample No. 35		Temperature : 500°C	
t(min)	Δm mg/mm ²	t(min)	Δm mg/mm ²		
0	0	300	1.42×10^{-3}		
30	4.76×10^{-4}	360	1.54×10^{-3}		
60	7.14×10^{-4}	420	1.67×10^{-3}		
90	9.52×10^{-4}	480	1.78×10^{-3}		
120	1.07×10^{-3}	540	1.90×10^{-3}		
180	1.19×10^{-3}				
240	1.31×10^{-3}				

Table 5.2		Sample No. 47		Temperature : 600°C	
0	0	300	3.5×10^{-3}		
15	8.3×10^{-4}	360	3.55×10^{-3}		
30	1.25×10^{-3}	420	3.95×10^{-3}		
60	2.49×10^{-3}	480	4.16×10^{-3}		
90	2.4×10^{-3}	540	4.37×10^{-3}		
120	3.12×10^{-3}	600	4.58×10^{-3}		
180	3.33×10^{-3}				
240	3.5×10^{-3}				

Table 5.3

Sample No. 42

Temperature : 700°C

t(min)	$\frac{\Delta m}{\text{mg/mm}^2}$	t(min)	$\frac{\Delta m}{\text{mg/mm}^2}$
0	0	180	2.81×10^{-3}
15	9.375×10^{-4}	240	3.43×10^{-3}
30	1.25×10^{-3}	300	3.75×10^{-3}
60	1.56×10^{-3}	360	4.063
90	1.875×10^{-3}		
120	2.19×10^{-3}		
150	2.5×10^{-3}		

Table 5.4

Sample No. 43

Temperature : 950°C

0	0	210	3.53×10^{-3}
15	5.4×10^{-4}	240	4.08×10^{-3}
30	8.1×10^{-4}	270	4.34×10^{-3}
45	1.08×10^{-3}	300	4.89×10^{-3}
60	1.63×10^{-3}	330	5.16×10^{-3}
90	1.90×10^{-3}	360	5.43×10^{-3}
120	2.17×10^{-3}	390	5.54×10^{-3}
150	2.45×10^{-3}	420	5.7×10^{-3}
180	2.99×10^{-3}	450	5.9×10^{-3}

Contd
Table 5 Contd..

VIII

Table 5.5		Sample No. 45		Temp.: 800° C	
t(min)	$\frac{\Delta m}{mg/mm^2}$	t(min)	$\frac{\Delta m}{mg/mm^2}$		
0	0	210	0.00594		
15	0.00937	240	0.00656		
30	0.00125	270	0.00686		
45	0.00188	300	0.00719		
60	0.0025	330	0.0075		
90	0.00313	360	0.00781		
120	0.00375	420	0.00875		
150	0.00438	540	0.00968		
180	0.00531	600	0.0103		

Table 5.6		Sample No. 33	Temp. 850°C
0	0	270	0.0105
30	0.00265	300	0.0108
60	0.00497	360	0.011
90	0.00635	420	0.0116
120	0.00714	480	0.0119
150	0.00767	540	0.0121
180	0.00847	600	0.0124
210	0.00899		
240	0.952		

Table 5.7

Sample No. 34

Temp.: 900° C

t(min)	Δm mg/mm ²	t(min)	Δm mg/mm ²
0	0	180	0.0105
15	0.00256	240	0.012
30	0.00410	300	0.0123
45	0.00512	360	0.0133
60	0.00615	390	0.0143
90	0.00769	420	0.0154
120	0.00923	450	0.0164
150	0.00999	480	0.0169

Table 5.8

Sample No. 39

Temp.: 950° C

0	0	120	0.0162
15	0.0032	150	0.0182
30	0.0064	180	0.0205
45	0.0091	210	0.0237
60	0.0104	240	0.0273
75	0.0114	270	0.0299
90	0.0123	300	0.033

Table 5.9	Sample No. 40	Temp. 1000° C
0	0	180
15	0.0038	210
30	0.0103	240
45	0.0136	270
60	0.0168	300
75	0.0195	360
90	0.0231	420
120	0.0337	480
150	0.0473	

TABLE NO. 6.

Thermogravimetric Data at 800° C for various surface finishes.

Table 6.1	Sample No. 36	belt	Polished
t(min)	Δm mg/mm ²	t(min)	Δm mg/mm ²
0	0	210	0.0107
15	0.00176	240	0.0118
30	0.00296	300	0.0136
45	0.00385	360	0.0154
60	0.00503	420	0.0168
90	0.00651	480	0.0176
120	0.00769	510	0.0183
150	0.0086		
180	0.00976		

Table 6.2		Sample No. 48	1/0 finish
0	0	180	0.00654
15	0.0019	210	0.0068
30	0.00208	240	0.00744
45	0.00238	270	0.0080
60	0.00297	300	0.00833
75	0.00327	330	0.0086
90	0.00416	360	0.0089
120	0.00535	390	0.00922
150	0.00654		

Table 6.3		Sample No. 45	4/0 finish
See table 5.5			

Table 6.4		Sample No. 51	Alumina Polished
0	0	240	0.00660
15	0.00069	270	0.00729
30	0.00104	300	0.00763
60	0.00208	360	0.00790
90	0.0027	420	0.00833
120	0.0038	480	0.00668
150	0.00451	540	0.00902
180	0.00521		
210	0.00590		

Table 6.5		Sample No. 52	Electro polished
0	0	240	0.00562
30	0.00208	300	0.0062
60	0.00291	360	0.00667
90	0.0033	420	0.00708
120	0.00417	480	0.00749
150	0.00458	540	0.00790
180	0.00499		
210	0.00541		

Table No. 7
Thermogravimetric Data

Table 7.1		Sample No. XXVI		Temperature: 600°C
Time (min.)	Weight gain (mg/mm ²)	Time (min)	Weight gain (mg/mm ²)	
0	0	240	2.35×10^{-3}	
15	5.88×10^{-4}	300	2.35×10^{-3}	
30	1.17×10^{-3}	360	2.35×10^{-3}	
45	1.76×10^{-3}			
60	2.05×10^{-3}			
90	2.15×10^{-3}			
120	2.35×10^{-3}			
180	2.35×10^{-3}			

Table 7.2		Sample No. XXV		Temperature: 700°C
0	0	360	5.58×10^{-3}	
30	8.8×10^{-4}	420	6.18×10^{-3}	
60	2.06×10^{-3}	480	6.47×10^{-3}	
90	2.65×10^{-3}	540	6.76×10^{-3}	
120	3.24×10^{-3}	600	7.35×10^{-3}	
150	3.82×10^{-3}	660	7.94×10^{-3}	
180	4.41×10^{-3}	720	8.53×10^{-3}	
240	4.99×10^{-3}			
300	5.29×10^{-3}			

Table 7.3		Sample No. XVI		Temperature : 800°C	
Time (min.)	Weight ₂ gain (mg/mm ²)	Time (min.)	Weight ₂ gain (mg/mm ²)	Time (min.)	Weight ₂ gain mg/mm ²
0	0	360	9.72×10^{-3}	840	0.0158
30	1.13×10^{-3}	420	0.0108	900	0.016
60	2.78×10^{-3}	480	0.0116	960	0.0166
90		540	0.0136	990	0.0172
120	4.99×10^{-3}	600	0.0141		
180	6.38×10^{-3}	660	0.0149		
240	8.06×10^{-3}	720	0.0152		
300	9.17×10^{-3}	780	0.0156		

Table 7.4		Sample No. XXII		Temperature: 900°C	
0	0	180	0.0138	660	0.0192
15	3.54×10^{-3}	240	0.0153	720	0.0194
30	6.49×10^{-3}	300	0.0159		
45		360	0.0171		
60	8.86×10^{-3}	420	0.0174		
90	0.0106	480	0.0180		
120	0.0118	540	0.0186		
150	0.0129	600	0.0189		

Table 7.5		Sample No. XX		Temperature: 950°C	
0	0	32	0.0134	150	0.0207
4	3.95×10^{-3}	36	0.0138	180	0.0215
8	6.81×10^{-3}	40	0.0145	240	0.0214
12	8.79×10^{-3}	44	0.0152	300	0.0224
16	9.89×10^{-3}	48	0.0154	360	0.0228
20	0.0109	60	0.0167	420	0.0235
24	0.0119	90	0.0193	480	0.0246
28	0.0127	120	0.0204	540	0.0250
				600	0.0257

Table 7.6		Sample No. XXII		Temperature: 1000°C	
0	0	40	0.0157	270	0.0445
4	4.24×10^{-3}	48	0.0167	300	0.0513
8	6.82×10^{-3}	60	0.0178	330	0.0583
12	8.23×10^{-3}	90	0.0211	352	0.0729
16	0.0103	120	0.0232	360	0.0756
20	0.0115	150	0.0256	390	0.0804
24	0.0124	180	0.0273	420	0.084
28	0.0134	210	0.0296	450	0.086
32	0.0143	240	0.0338	480	0.089
				540	0.097
				600	0.099

Table No. 8

Table 8.1		Sample No.: P6		Oxygen Pressure: 240 mm	
Time (min.)	Weight gain (mg/mm ²)	Time (min.)	Weight gain (mg/mm ²)	Time (min.)	Weight gain (mg/mm ²)
0	0	150	6.25×10^{-3}	540	0.0112
15	1.25×10^{-3}	180	6.56×10^{-3}	560	0.0118
30	2.19×10^{-3}	240	6.87×10^{-3}		
60	3.75×10^{-3}	300	7.5×10^{-3}		
90	4.68×10^{-3}	360	8.12×10^{-3}		
120	5.62×10^{-3}	420	8.75×10^{-3}		
		480	0.01		

Table 8.2		Sample No. P9		Oxygen Pressure : 360 mm	
0		180	9.80×10^{-3}		
15	8.40×10^{-4}	240	0.0117		
30	2.24×10^{-3}	300	0.0131		
60	4.48×10^{-3}	360	0.0148		
90	5.32×10^{-3}	420	0.0162		
120	7.28×10^{-3}	480	0.0170		
150	8.12×10^{-3}	540	0.0176		
		600	0.0182		

Table 8.3		Sample No. P10		Oxygen Pressure : 460 mm	
0	0	240	0.0106		
15	1.47×10^{-3}	300	0.0112		
30	2.35×10^{-3}	360	0.0132		
60	3.82×10^{-3}	420	0.0141		
90	4.70×10^{-3}	480	0.0149		
120	6.17×10^{-3}	540	0.0107		
150	8.82×10^{-3}	600	0.0176		
180	9.4×10^{-3}				

Table 8.4		Sample No. P4		Oxygen Pressure : 530 mm	
0	0	120	9.59×10^{-3}	560	0.0192
4	1.54×10^{-3}	180	0.0117		
8	2.47×10^{-3}	240	0.0133		
12	4.33×10^{-3}	300	0.0148		
16	4.95×10^{-3}	360	0.0161		
30	5.26×10^{-3}	420	0.0170		
60	6.81×10^{-3}	480	0.0183		
90	8.67×10^{-3}	540	0.0192		

Table 8.6		Sample No. P8	Oxygen Pressure: 760 mm
0	0	240	0.0138
15	2.2×10^{-3}	300	0.016
30	3.88×10^{-3}	360	0.0183
60	7.22×10^{-3}	420	0.0203
90	8.33×10^{-3}	480	0.0211
120	9.94×10^{-3}	540	0.0227
150	0.110	600	0.0233
180	0.0116		

Table No. 9					
Table 9		Sample No. W5	Temperature: 650°C		
Time (min.)	Weight gain (mg/mm ²)	Time (min)	Weight gain (mg/mm ²)	Time (min.)	Weight gain (mg/min ²)
0	5.56×10^{-4}	360	6.66×10^{-3}	900	9.58×10^{-3}
30	1.1×10^{-3}	420	7.49×10^{-3}	960	9.72×10^{-3}
60	1.67×10^{-3}	480	8.05×10^{-3}	1020	9.86×10^{-3}
90	2.22×10^{-3}	540	8.33×10^{-3}	1060	9.99×10^{-3}
120	3.33×10^{-3}	600	8.61×10^{-3}		
180	4.99×10^{-3}	660	8.74×10^{-3}		
240	6.11×10^{-3}	720	8.88×10^{-3}		
300	6.66×10^{-3}	780	9.16×10^{-3}		
		840	9.30×10^{-3}		

Table 9.2		Sample No. W1		Temperature: 750°C	
0	0	240	8.33×10^{-3}	720	0.0163
30	1.67×10^{-3}	300	9.72×10^{-3}	780	0.0169
45	2.78×10^{-3}	360	0.0105	840	0.0172
60	3.61×10^{-3}	420	0.0119	900	0.0175
90	4.72×10^{-3}	480	0.0133	960	0.0178
120	6.11×10^{-3}	540	0.0142	1020	0.0180
150	6.94×10^{-3}	600	0.0149	1080	0.0188
180	7.49×10^{-3}	660	0.0115		

Table 9.3		Sample No. W2		Temperature: 850°C	
0	0	180	0.0238	600	0.0542
4	1.70×10^{-3}	210	0.0247	660	0.0656
16	4.82×10^{-3}	240	0.0249	720	0.0756
24	8.23×10^{-3}	300	0.026	780	0.0863
32	9.66×10^{-3}	360	0.0278	840	0.0954
48	0.0108	420	0.0308	900	0.1056
60	0.0122	480	0.0340	960	0.1272
90	0.0159	510	0.0378	1020	0.160
120	0.020	540	0.0426		
150	0.0224	570	0.0482		

Table 9.4		Sample No. W8		Temperature: 850°C	
0	0	240	0.0128		
15	1.66×10^{-3}	300	0.0138		
30	3.88×10^{-3}	360	0.0149		
45	5.83×10^{-3}	420	0.0161		
60	6.39×10^{-3}	480	0.0169		
90	8.05×10^{-3}	540	0.0172		
120	9.99×10^{-3}	600	0.0178		
150	0.0108	660	0.0194		
180	0.0111	1080	0.0366		

Table 9.5		Sample No. W3		Temperature: 950°C	
0	0	180	0.0243	660	0.0336
6	4.81×10^{-3}	210	0.0248	720	0.0347
10	8.02×10^{-3}	240	0.0259	780	0.0352
18	0.0133	300	0.0267	840	0.0363
30	0.0152	360	0.0278	900	0.0379
42	0.0171	420	0.0287	960	0.0395
60	0.0189	480	0.0299	1020	0.0409
90	0.0208	540	0.0315	1080	0.0422
120	0.0214	600	0.032		
150	0.0232				

Table 9.6		Sample No. W4		Temperature: 1000°C	
0	0	60	0.0378	304	0.126
4	0.0111	90	0.049	308	0.137
8	0.0138	120	0.0636	312	0.1538
12	0.0156	150	0.0752	320	0.168
16	0.0186	180	0.0822	330	0.175
20	0.0205	210	0.0933	360	0.191
32	0.0238	240	0.1019	390	0.202
40	0.0272	270	0.1099	420	0.207
48	0.0305	300	0.1205	480	0.212

APPENDIX 2

X-ray Diffraction Data for some important compounds

Compound	'd' values			I/I ₁ ratio			Card No.
α -Fe ₂ O ₃	2.69	1.69	2.51	100	60	50	13-534
γ -Fe ₂ O ₃	2.52	2.95	1.61	101	101	101	15-615
Fe ₃ O ₄	2.53	1.61	1.48	100	85	85	11-614
FeO	2.15	2.49	1.52	100	80	60	6-615
α Fe ₂ O ₃ ·H ₂ O	4.21	2.69	2.44	100	80	70	18-97
FeCr ₂ O ₄	2.51	1.91	1.61	100	75	75	4-759
FeMoO ₄	2.88	1.68	3.56	100	70	40	16-326
MoO ₂	3.41	2.42	1.70	100	85	80	5-0452
MoO ₃	3.26	3.81	3.46	100	82	61	5-508
(Cr,Fe) ₂ O ₃	1.68	3.63	2.69	100	80	80	2-1357
Cr ₂ N	2.10	2.38	2.22	100	25	25	1-1232
CrN	2.07	2.39	1.46	100	80	80	11-65
Cr ₂ O ₃	2.67	2.48	1.67	100	96	90	6-504
CrO ₂	3.11	1.63	2.42	100	75	60	9-332
CrO ₃	4.16	3.42	3.36	100	100	100	9-47

Colour of Various Oxides

Cr_2O_3	- green
$\text{Cr}_2\text{O}_3 \times \text{H}_2\text{O}$	- violet, bluish green
CrO	- Black
CrO_2	- Brown black
MoO_2	- lead grey
Mo_2O_3	- black
MoO_3	- whitish-yellow
$\text{Fe}_2\text{N}, \text{Fe}_4\text{N}$	- grey
FeO	- black
Fe_2O_3	- red, brownish-black
$\text{Fe}_2\text{O}_3 \times \text{H}_2\text{O}$	- red-brownish
Fe_3O_4	- black